Deep-Sea Research, Vol. 38, Suppl. 1, pp. S411–S443, 1991.
Printed in Great Britain.

0198-0149/91 $3.00 + 0.00

A deep-reaching anticyclonic eddy in the subtropical gyre of the eastern South Atlantic

M. S. McCartney* and M. E. Woodgate-Jones*

(*Received* 16 *August* 1989; *in revised form* 30 *October* 1990; *accepted* 5 *November* 1990)

Abstract—A CTD transect of the South Atlantic at a nominal latitude of 23°S was made in early 1983. About two-thirds of the way from the Brazil Current in the west to the Benguela Current in the east, we encountered a large-diameter eddy (300–400 km). Its dynamic signature (bowl-shaped isopycnals) penetrated to over 4000 m, with the eddy anticyclonic transport relative to 4000 db over 30×10^6 m^3 s^{-1}. Various origins for this eddy are conceivable. We feel that the most likely one is the Agulhas Retroflection region: that the eddy was formed by a pinching off of this current elbow, and a subsequent northwest movement of more than 2500 km over a period spanning two winters. There was a superposed double thermostad in the core of the eddy interpreted to be the product of two successive winters' convective overturning. Main thermocline waters from the Agulhas Current, recognizable by the distribution of oxygen, were trapped in the eddy core and carried with it. This trapping could extend as deep as the Antarctic Intermediate Water (AAIW). The propagating eddy distorted the local property distributions. A ring of low-oxygen water from lower latitudes surrounded the core of the eddy at the thermocline levels. AAIW of higher salinity and lower oxygen, and Deep Water of higher salinity and lower nutrients were observed at the eddy stations. These characteristics are also found to the north of the eddy. The kinematics of a drifting anticyclonic eddy provides a framework for understanding the trapping, the low-oxygen ring, and the pulling underneath of the AAIW and Deep Water.

1. OBSERVATIONAL BACKGROUND

In early 1983 a transect of the South Atlantic was made (R.V. *Oceanus* Cruise 133, 4 February–5 March, 1983) between Rio de Janeiro, Brazil, and Walvis Bay, Namibia (nominally 23°S, Fig. 1). A total of 86 full water depth CTD stations were made, with up to 24 supportive water samples per station (salinity and oxygen measurements for calibration of profiles, and nutrient measurements: SiO_2, NO_2, NO_3 and PO_4). The purpose of the present paper is to report an observation of an energetic mesoscale eddy in the transect and to speculate on its origin.

The distributions of properties along the transect are shown in Fig. 2. For orientation, the following general circulation features should be noted:

(1) An onshore uplifting of isotherms warmer than 10°C near the western boundary associated with the (southward-flowing) Brazil Current (Fig. 2a).

(2) A gentle west-to-east rise of isotherms warmer than 5°C from immediately offshore of the Brazil Current all the way east to Africa, indicative of the broad northward flow of the subtropical gyre's interior (Fig. 2a).

*Woods Hole Oceanographic Institution, Woods Hole, MA 02543, U.S.A.

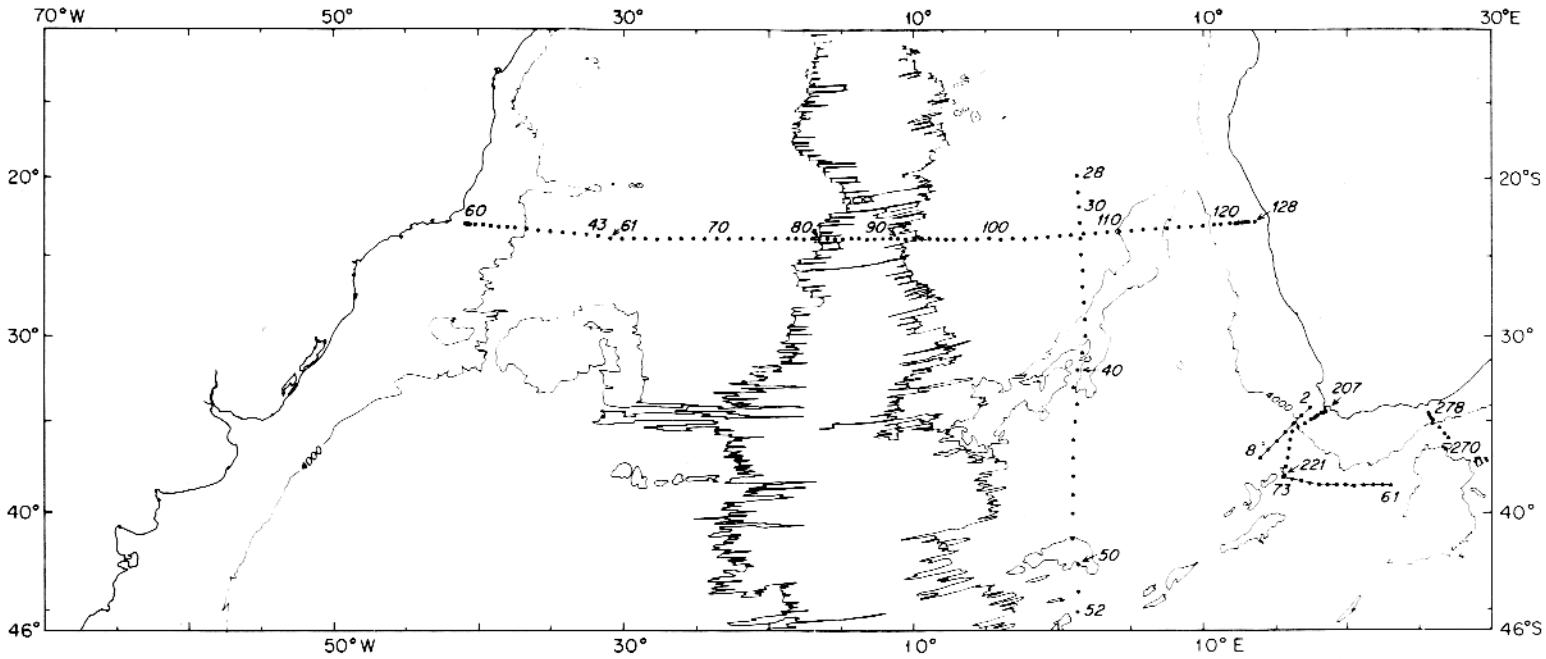

Fig. 1. Coast lines and 4000-m isobath (after HEEZEN and THARP, 1978) for the southern South Atlantic. Line segments show the locations of sections used in subsequent figures.

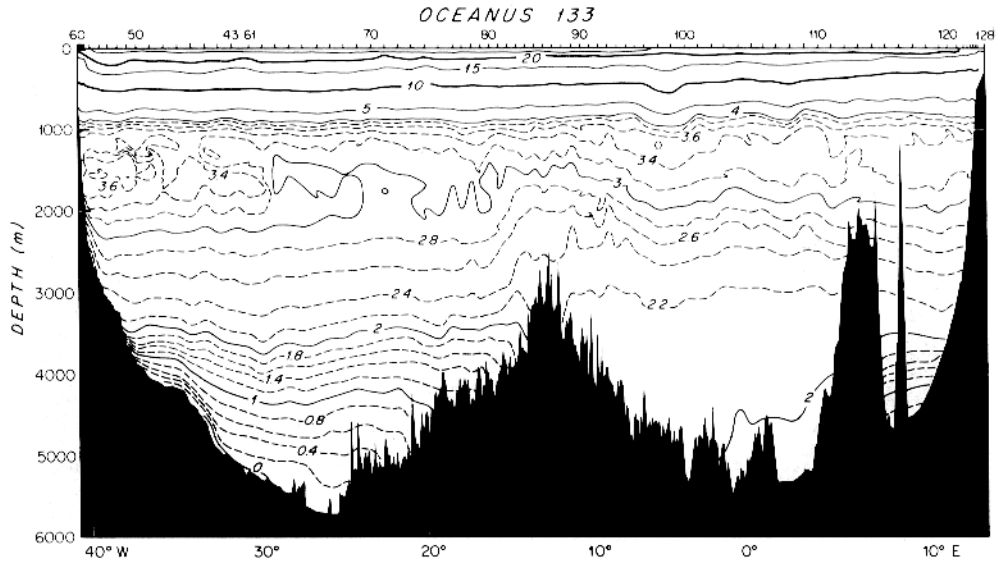

(a)

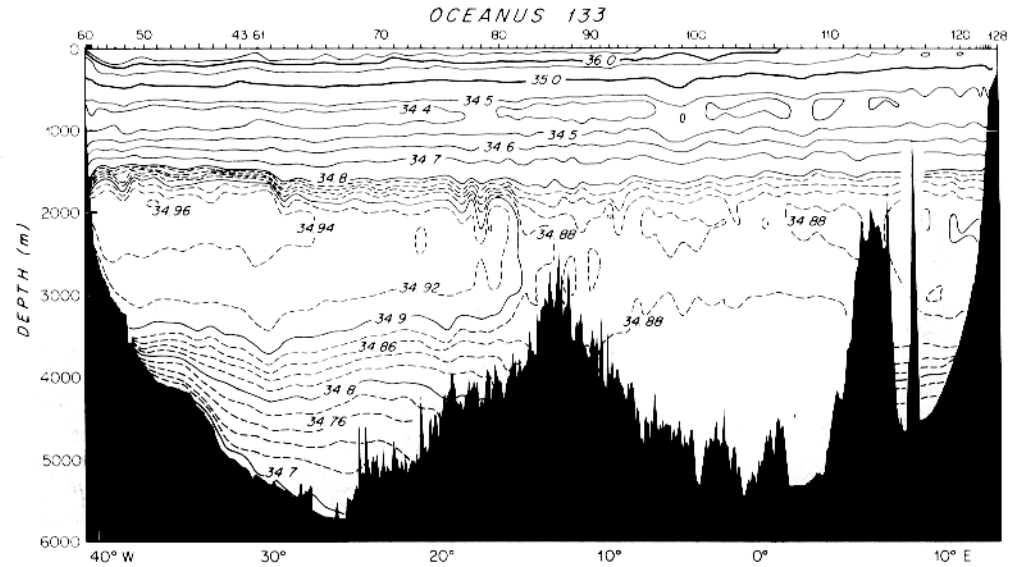

(b)

Fig. 2. Property distributions at nominally 23°S, R.V. *Oceanus* Cruise 133, legs 3 and 4, February–March, 1983. Transect position in Fig. 1. (a) Potential temperature (°C); (b) salinity (psu). (*Continued overleaf*)

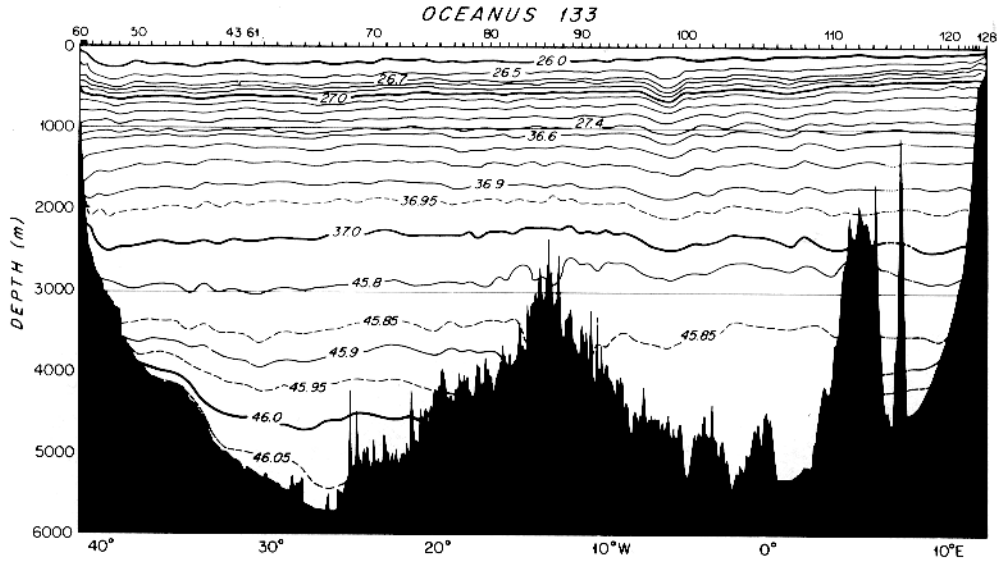

(c)

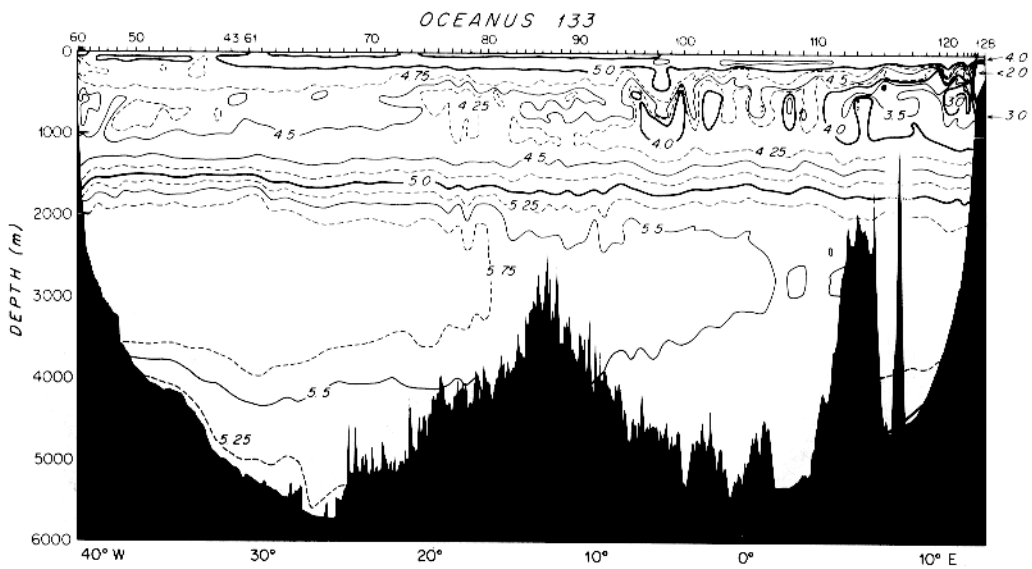

(d)

Fig. 2 *continued*. (c) Potential density anomaly, referenced to 0, 2000 and 4000 db (kg m^{-3}); (d) dissolved oxygen (ml l^{-1}); (e) dissolved silica (μmol l^{-1}); (f) dissolved nitrate (μmol l^{-1}).

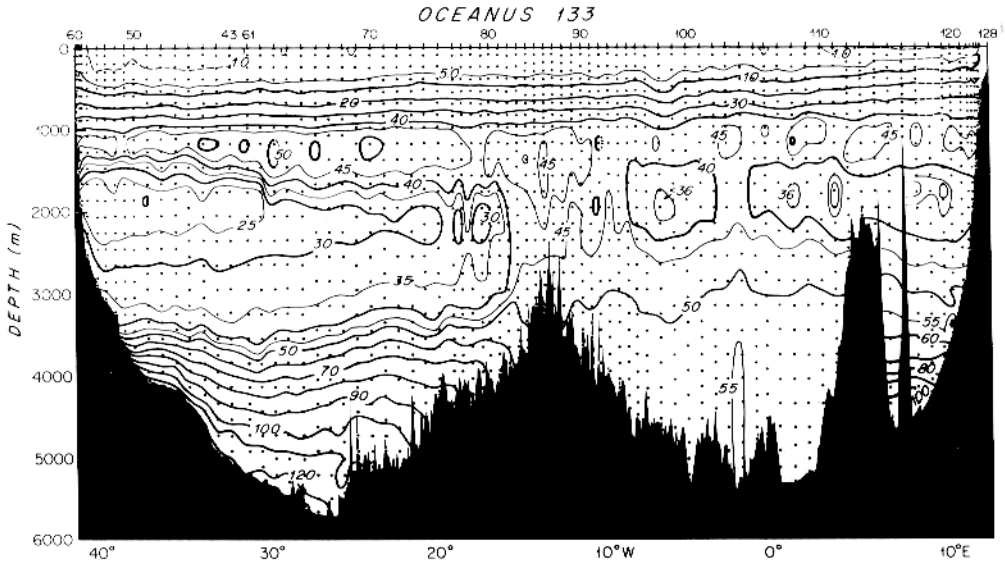
OCEANUS 133
DEPTH (m)
40°
30°
20°
10°W
0°
10°E

(e)

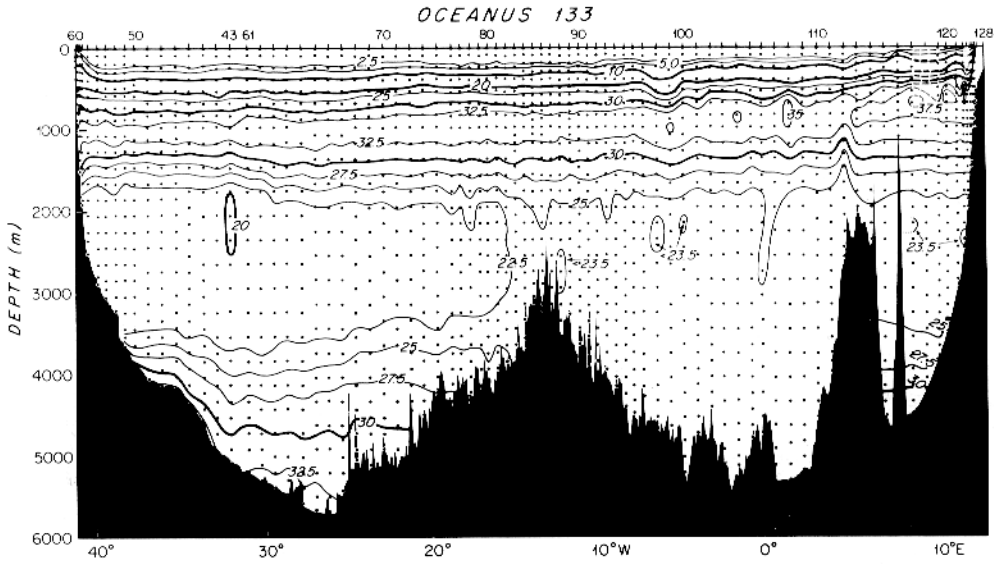
OCEANUS 133
DEPTH (m)
40°
30°
20°
10°W
0°
10°E

(f)

(3) A western-intensified temperature inversion in the depth range 1000–2000 m, the signature of the layering of the relatively fresh Antarctic Intermediate Water (AAIW) of southern origin near 1000 m and the relatively saline North Atlantic Deep Water (NADW) of northern origin near 2000 m (Fig. 2b).

(4) A strong offshore downslope of isotherms colder than 2°C near the western boundary indicating the western-intensified northward flow of Antarctic Bottom Water (Fig. 2a).

(5) A doming of isotherms colder than 3.5°C over the crest of the Mid-Atlantic Ridge, perhaps indicative of an interaction between the basin-scale interior circulation and the north–south trending Ridge (*à la* Joyce, 1981) (Fig. 2a). A distinct water mass front in the Deep Water occurs in the neighborhood of the Ridge crest (Fig. 2b,d,e,f).

(6) Weak stratification in the abyss between the Mid-Atlantic Ridge and the Walvis Ridge, indicative of the limited sources of deep water for this region (predominantly equatorial zone sources; see Warren, 1981 and Warren and Speer, 1990) (Fig. 2a,c).

(7) Colder water and increased abyssal stratification between the Walvis Ridge and the coast of Africa indicative of the connectedness of this basin to cold water sources in the south (Fig. 2a,c).

Against these general circulation and large-scale background features can be seen various smaller scale structures. The most coherent structure is a depression in the thermocline centered at Stas 98 and 99, overlying the base of the east flank of the Mid-Atlantic Ridge (Fig. 2a). The isotherm "bowl" is about 100–150 m deep and spans about a 300-km width. Lacking data in the third spatial dimension, we cannot be certain, but it seems unlikely, that this could be an elongated filamentary structure in mid-ocean. We thus suppose that this structure is an eddy of some sort—i.e. that it is roughly symmetric about an axis of rotation—and we shall identify it as simply "the eddy" for the rest of this paper. The maximum depth of the 10°C isotherm at the middle of the eddy is about 550 m. The only other location on the entire transect where the 10°C isotherm reaches close to this depth is immediately offshore of the Brazil Current.

The eddy is superimposed on the general west-to-east rise of isotherms amounting to 150 m between the Ridge crest and the coast of Africa (Fig. 2a). This broad rise is otherwise smooth except for a less pronounced bowl near Stas 107 and 108, a possibly related structure discussed below. The overall thermocline rise eastward from Sta. 51, the edge of the Brazil Current, represents the broad scale interior circulation. From Sta. 51 east to the coast of Africa, the integrated northward transport in the interior above 1300 db (or the bottom if shallower), using that surface as a level of no-motion (after Warren and Speer, 1990), is 29×10^6 m^3 s^{-1}. With this level of no-motion, the Brazil Current, Stas 60–51, has an integrated southward transport of 11×10^6 m^3 s^{-1}. The anticyclonic transport of the eddy, calculated in the same way, is about 17×10^6 m^3 s^{-1}, and thus is a disturbance of a magnitude comparable to that of the permanent components of the general circulation. Table 1 summarizes the transports on the two sides of the eddy for a selection of levels of no-motion, to facilitate later comparisons to other observations.

The penetration depth of the eddy is remarkable, indicating a deep-reaching geostrophic signature (Fig. 2c). Below the isopycnal slope reversal near 200 m, the geostrophic shear is esentially monotonic and non-zero all the way down to the abyss. To quantify the depth extent of this shear, Fig. 3 shows profiles of velocity normal to the section computed relative to an assumed (arbitrary) level of no-motion at 4000 db for the two station pairs defining the eddy maximum speeds. While speeds drop below ± 5 cm s^{-1} below 1100 db, a

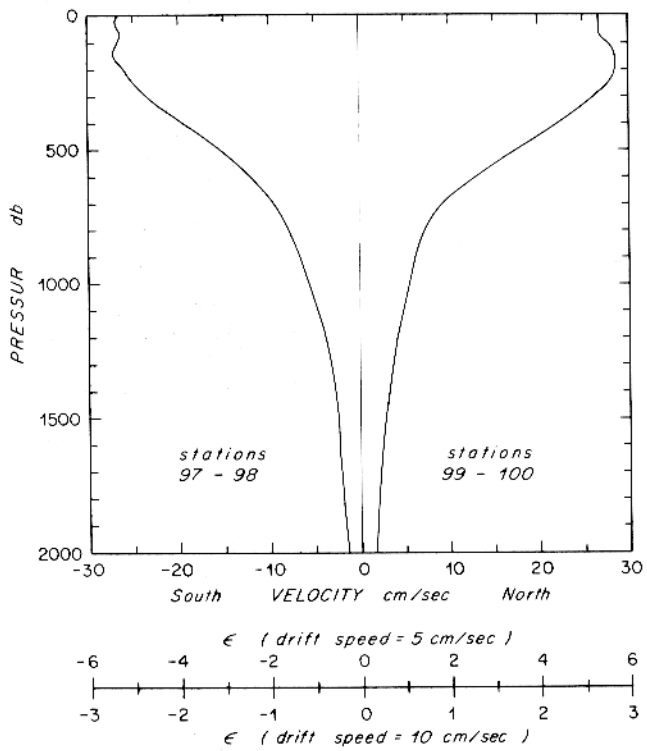

Fig. 3. Velocity profiles for the station pairs defining the eddy maximum azimuthal speed, calculated by geostrophy for a level of no-motion at 4000 db. The second axis gives Flierl's evaporometer for two choices of eddy drift speed.

sizable fraction of the eddy anticyclonic transport (25%) is found below 1100 db. The northward transport is antisymmetric for the two sides, an indication that this structure actually is an eddy—and a strong one at 35×10^6 m^3 s^{-1} (relative to 4000 db, Table 1).

The eddy has no obvious surface signature in this section, but the near-surface thermal field is rather peculiar (Fig. 4a). The isotherm bowl is quite noticeable below 300 m, and involves the 15°C and colder isotherms. This bowl is "filled" by a thermostad at 15–16°C, so

Table 1. *Volume transport in* 10^6 m^3 s^{-1} *for the two sides of the eddy, above the indicated levels of no-motion, in the indicated directions north* (*N*) *or south* (*S*)

Level of no-motion	Station groups			
	95–99	96–99	99–102	99–103
1100 db	13.9 S	14.5 S	15.2 N	14.4 N
1300 db	16.6 S	17.1 S	17.4 N	17.1 N
1500 db	19.1 S	19.3 S	19.2 N	19.8 N
4000 db	36.2 S	32.5 S	30.0 N	35.3 N

that the 16 and 17°C isotherms are more or less flat. A second thermostad occurs between 17 and 18°C, resulting in a dome rather than a bowl in the isotherms between 18 and 22°C (Fig. 4a,b). Accompanying this change in isotherm slope is a change of sign in the geostrophic shear. At the base of and beneath the thermocline, isotherms continue to show the bowl shape, but the width of the bowl appears to increase, from 300 km at 500 m, to 400 km at 700 m, to 600 km and more below 1400 m. This is to some degree an artifact of the interplay between temperature and salinity (Fig. 4b,c), for the density field (Fig. 4d) shows less width change: from 300 km at shallow levels to 400 or 450 km at deeper levels (actually we can just say less than 480 km given the spacing of our stations beneath XBT depth).

There is a shift in the temperature/salinity relationship for stations within the eddy compared to those outside of it. This shift is reflected in the non-parallelism of isotherms, isohalines and isopycnals (Figs 2b,c,d and 4a,b,c), spanning the low salinity stratum of the Antarctic Intermediate Water (AAIW), from about $\theta = 6.0$°C to nominally $\theta = 3.0$°C, and the higher salinity stratum of the Upper North Atlantic Deep Water (UNADW) down to a temperature of about $\theta = 2.4$°C. The salinity minimum near 800 m (Fig. 4c) that defines the core layer for the AAIW is not as strong inside the eddy as outside: the eddy has saltier AAIW. This relatively saline mid-depth temperature/salinity relationship extends much deeper than just the salinity minimum core. Comparing the fields of temperature (Fig. 4b) to salinity (Fig. 4c), the isohalines are much flatter than the isotherms below 1000 m. The water inside the eddy is saltier than that outside on isotherms colder than about 6°C. Deeper in the water column, the salinity maxima of the UNADW is slightly more saline so that there is a closed salinity contour (34.88 psu) centered at the eddy at a depth of 2200 m (Fig. 2b).

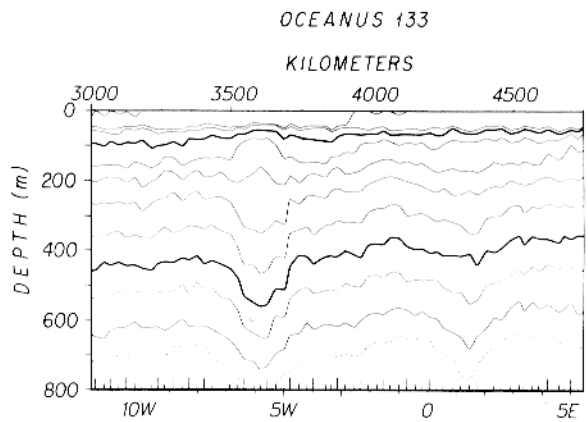

(a)

Fig. 4. Upper water column detailed property distributions at nominally 23°S (same cruise data as Fig. 2). (a) *In situ* temperature (°C) merged XBT (short tickmarks) and CTD (long tickmarks) profiles; (b) potential temperature (°C); (c) salinity (psu).

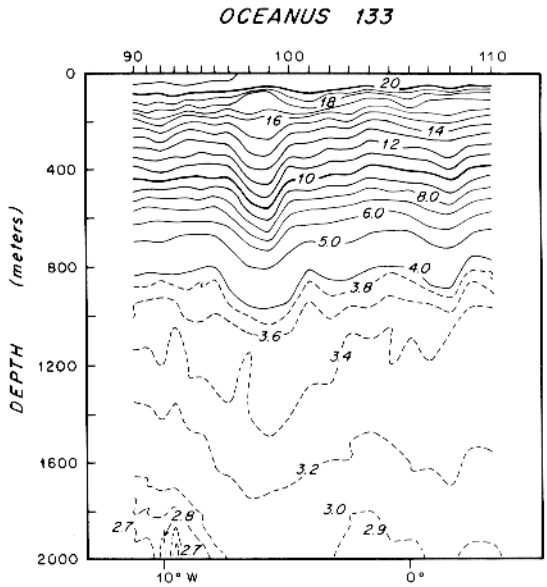
OCEANUS 133
90
100
110
0
400
800
1200
1600
2000
DEPTH (meters)
20
18
16
14
12
10
8.0
6.0
5.0
4.0
3.8
3.6
3.4
3.2
3.0
2.9
2.8
2.7
2.7
10° W
0°

(b)

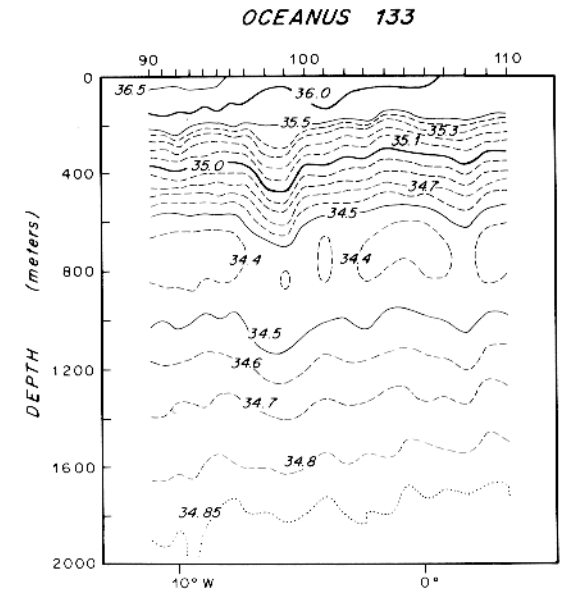
OCEANUS 133
90
100
110
0
400
800
1200
1600
2000
DEPTH (meters)
36.5
36.0
35.5
35.3
35.1
35.0
34.7
34.5
34.4
34.4
34.5
34.6
34.7
34.8
34.85
10° W
0°

(c)

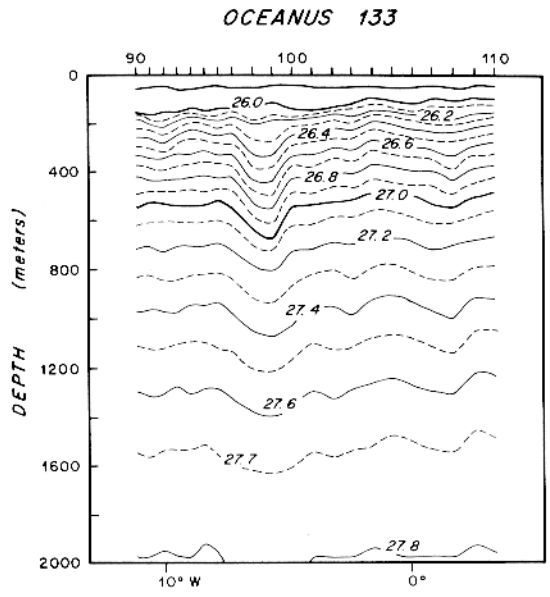

(d)

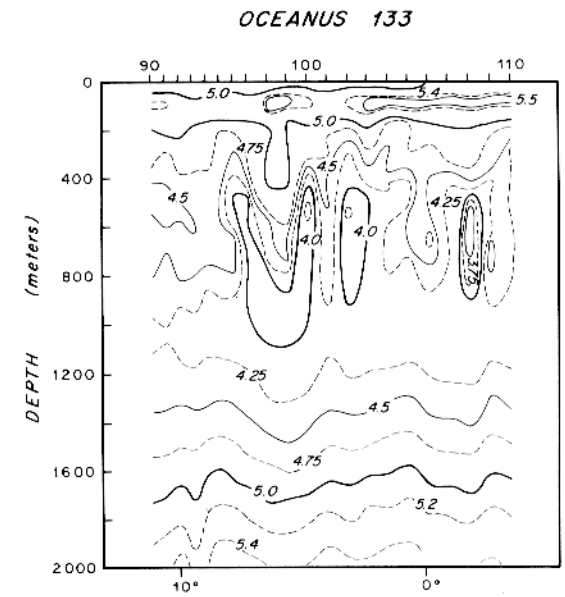

(e)

Fig. 4 *continued*. (d) Potential density anomaly, referenced to 0 db (kg m^{-3}); (e) dissolved oxygen (ml l^{-1}).

Additional anomalous water mass characteristics are revealed by the oxygen section (Fig. 4d). In the eddy core these oxygen anomalies bridge the temperature range from the lower thermostad through the AAIW core. At stations well outside the eddy, there is generally an oxygen maximum layer ($\geq$4.5 ml l^{-1} and occasionally $\geq$4.75 ml l^{-1}) coincident with the core layer of the AAIW, with a minimum layer ($\leq$4.5 ml l^{-1}) beneath it centered on a temperature of about 3.8°C, a minimum layer ($\leq$4.5 ml l^{-1}) at mid-thermocline near $\theta = 8$°C, and oxygen higher than 5.0 ml l^{-1} restricted to the upper thermocline above about 200 m ($\theta \geq 15$°C). In both the peripheral stations (97 and 100) and the central stations (98 and 99) of the eddy, the AAIW core has lower oxygen levels and is no longer an oxygen maximum layer. The oxygen minimum layer that outside the eddy is below the AAIW core and centered on $\theta = 3.8$°C expands in thickness within the eddy, and centers on the AAIW core. The central stations thus actually have an oxygen minimum layer ($\leq$4.25 ml l^{-1}) near the AAIW core.

Above the AAIW the central stations show a completely different oxygen layering than the peripheral stations, which are in turn different from the surrounding stations. For the central stations the elevated oxygen levels ($\geq$5.0 ml l^{-1}) extend downward to below 400 m to a temperature of about 12°C, compared to 15°C on the outside. Highest oxygen levels are found at the uper thermostad, a second maximum centered near 13.5°C, and from there downward a monotonic decline to the oxygen minimum just below the core of the AAIW ($\theta = 3.5$°C) is observed. The peripheral stations exhibit a steady decrease of oxygen downward from the near-surface maximum found throughout the section to an extreme low ($\leq$4.0 ml l^{-1}) at 6–10°C, then an increase down into the deep water, but with some indication of a weak maximum reappearing at the AAIW core near 4.5°C. The eddy thus has a ring of very low-oxygen water surrounding the higher oxygen core water mass at main thermocline depths.

In the deep water the Mid-Atlantic Ridge seems to perturb all isopycnals below about 2000 m (Fig. 2c). Particularly curious is how isopycnals "dive" down to the ridge flank in a band of about 300 m thickness and about 100–200 km width. The deep footprint of the eddy merges with this band near 4000 m, so the eddy may be feeling topographic steering effects, although it is centered 750 km east of the ridge crest. We further note that outside of the aforementioned band of diving isopycnals, there appears to be a 1200-km wide dome in the isopycnals below 1500 m centered at the ridge crest to further complicate the interpretation. The western edge of the dome seems associated with a frontal transition of deep water properties from western basin to eastern basin character (Fig. 2b,d,e,f), and not to have any manifestation shallower than about 1500 m. The eastern edge of the dome, on the other hand, coincides with the western half of the deep footprint of the large eddy, which is coherent with an upper ocean feature.

There are some differences in the nutrient distributions in the deep water eddy footprint compared to the immediate stations to either side, including those in the east half of the dome over the Ridge (Fig. 2e,f). For example, the silicate maximum layer (near 1200 m) beneath the AAIW core is not as strong within the eddy as in the surrounding stations. Deeper down at the eddy-intensified salinity maximum core of the UNADW, the silicate minimum is more pronounced within the eddy footprint than outside ($\leq$36 μmol l^{-1}, Fig. 2e), and immediately below this the related broader nitrate minimum is stronger too ($\leq$23.5 μmol l^{-1}, Fig. 2f).

The explanation of the eddy should take into account these deep water features as well as the AAIW and thermocline anomalies. One possibility is that deep water is also

dynamically trapped within the eddy, and thus represents a water mass carried with the eddy from its point of formation. We will conclude later that the trapping is unlikely to penetrate this deep, even though the dynamic signature of the circulation does. The deep water patterns instead represent a distortion by the eddy of the pattern of strong meridional property gradients in the deep water that are found in this region.

Before discussing possible origins of this eddy, we note the possibility of another eddy or related feature in the section, near Sta. 108. The temperature and density sections (Fig. 4a,b,d) show a shallower and less symmetric bowl there, overlain by a weak thermostad (16–17°C temperature layer). This bowl, too, extends across the thermocline and shows the AAIW with elevated salinity and depressed oxygen (Fig. 4c,e) that characterized the first eddy. The details of Sta. 108 most resemble the peripheral stations (97 and 100) of the eddy, particularly the occurrence of very low oxygen in the thermocline. Our guess is that we crossed this feature off-center, thus missing its core. The total transport relative to 4000 db is about 16×10^6 m^3 s^{-1}—about half that of the first feature (consistent with an off-center crossing of an eddy of comparable strength). The southward transport occurs over three station pairs (105–108, total distance 234 km, transport 15.4×10^6 m^3 s^{-1}) while the northward transport is narrower, through one pair of stations (108–109, spaced at 87 km, transport 16.6×10^6 m^3 s^{-1}). There is a local maximum in isopycnal depth down to about 3500 m at Sta. 108, without nearly such a dramatic-looking footprint as the large eddy. Overall, this second eddy is not as large nor as well-defined as the strong eddy at 23°S, 5°W.

2. THE ORIGIN OF THE EDDY

There are several possibilities for the origin of the strong eddy and we will discuss them in order of increasing distance of the eddy from the possible generation site.

A. In situ *formation near the site of observation*

Upper ocean pycnostads are often products of winter convective overturning. This process was suggested by Worthington (1972) as an anticyclogenic process: that convection pushes down the thermocline causing baroclinic anticyclonic circulation about the site of deepest convection. Some evidence of this process was later found in the Gulf Stream Recirculation (Worthington, 1977; Leetmaa, 1977), which included documentation of a mesoscale eddy-like aspect to the convection events and resultant anticyclonic circulation. The mesoscale aspect may reflect the narrowness of the Gulf Stream Recirculation rather than a scale selection by the convection process. This is a mechanism that creates anticyclonic features within an anticyclonic gyre, which is one of the principal aspects of our eddy. But we doubt this as a viable mechanism for our eddy: the double pycnostad structure is problematic, and anticyclogenesis is usually thought of as an incremental increase to an existing anticyclone rather than creating one (particularly one with as much energy as this one). It is hard to imagine how the large-scale atmospheric forcing could form such a small-scale feature unless there was some preconditioned state of that small scale. The 24°S IGY section (Fuglister, 1960) was made in early spring and suggests that shallow convective overturning does occur at 17°C, the temperature of the shallow thermostad at the location where our eddy was observed. Furthermore, at 2°E, where we noted a second possible eddy with a 16°C thermostad, the IGY section shows a 16°C

shallow mixed layer, rather than deep convection. We are unable to find any evidence that convection at this latitude reaches the depth and/or temperature of the cooler thermostad (about 250 m).

Local convection in winter could be responsible for the near-surface thermostad but its depth presumably reflects the pre-existing bowl of the eddy rather than the convection creating the bowl. It seems likely that the deeper thermostad is of more remote origin. Further evidence of a remote rather than local origin for the eddy is the anomalous character of the water mass below the thermostads. The eddy contains in its center a broad high-oxygen layer spanning the thermocline, and this water mass is not found in the immediate neighborhood of our observations. Thus, local formation of this eddy does not appear to be viable.

B. The Brazil Current

Thermocline depths offshore of the Brazil Current are deep enough (Fig. 2) to account for the isotherm depth in mid-eddy without requiring further intensification or spin-up of the eddy as it hypothetically drifted eastward. In the 23°S section, the Brazil Current is restricted to depths shallower than 800 m judging from the tilt of the isopycnals. Deeper there are several slope reversals at the western boundary associated with the layered counterflows of the deep western boundary currents. Farther south as the Brazil Current axis trends to deeper water, top-to-bottom unidirectional shear develops (ZEMBA, in preparation), and an eddy formed from closing a piece of this system would have the deep baroclinic signature of our eddy. Indeed, the general circulation of the southwest corner of this subtropical gyre does resemble a large anticyclonic eddy, since the pronounced deepening to the south of the maximum depth of the thermocline implies a set of closed dynamic height contours on a scale of a few hundred kilometers preparation. The dynamic height difference across this compact recirculation gyre is more than ample to provide a baroclinic transport of 35×10^6 m^3 s^{-1} relative to a deep level of no-motion. Within this compact recirculation gyre, deep convection does occur (MCCARTNEY, 1977, 1982), producing a thermostad at temperatures close to that of the lower thermostad of our eddy. But otherwise there is no particular relationship between this gyre's water masses and those within our eddy. The Brazil Current gyre has oxygen maxima at the thermostad and at the core of the AAIW, and the thermocline between them exhibits a broad oxygen minimum. In the eddy, the oxygen minimum is much deeper, centered on the AAIW rather than mid-thermocline. The salinity minimum of the AAIW core in the neighborhood of the Brazil Current is the lowest of the entire subtropical gyre, while the eddy contains a saline variety of AAIW.

The formation mechanism is also problematic: a meander mechanism for eddy generation by a western boundary current of a subtropical anticyclonic gyre produces cyclonic eddies in the anticyclonic gyre interior. Anticyclonic eddies would be produced by shoreward meanders of the current, and would be found inshore of the current, not offshore. How would a pinched-off anticyclonic eddy make its way across the current back into the subtropical gyre? How would the compact recirculation gyre decouple itself from the Brazil Current and Brazil–Falkland confluence that are its western and southern quadrants, if it is this entire compact feature that propagated eastward?

The lack of a formation mechanism and the lack of water mass correspondence are powerful arguments against the Brazil Current as a source of the eddy.

C. The Benguela Current and southeast Atlantic

The Benguela Current is an upper ocean eastern-boundary current flowing northward along the coast of Africa (Hart and Currie, 1960) and crossing the 23°S section at 13°E (Fig. 2). It is not a very energetic feature in the section, and a formation mechanism for the strong eddy is therefore problematic. On the other hand, some aspects of the water mass relationships in the eddy are similar to those at the eastern end of the section. Fuglister's (1960) temperature and salinity sections at 24°S in early spring show surface mixed layers at the temperature range of the thermostads in the eddy. The thermocline oxygen distribution only partially matches: the low values found in the periphery of the eddy match, but the elevated oxygen in the eddy center between 10 and 15°C seems to have no counterpart near the Benguela Current (Fig. 2d). The salinity and oxygen values for the AAIW in the Benguela Current area are similar to those of the eddy core: more saline and lower in oxygen (Fig. 2b,d). Also, the NADW matches quite well in its elevated salinity and lowered silicate (Fig. 2b,d).

These similarities may imply some prior interaction between the eddy and the Benguela Current region, but there is not an obvious mechanism for spawning such an energetic eddy directly from the Benguela Current, which at this latitude is simply baroclinically too weak.

D. The Agulhas Current Retroflection

Formation of the eddy in the Agulhas Current Retroflection is an attractive possibility, since the current involved is amply energetic to spawn an anticyclonic eddy with baroclinic transport as large as observed in the eddy. The Agulhas Current retroflects or turns back on itself south of Africa, over a typical radius of a few hundred kilometers. When this anticyclonic retroflection pinches off, like a Gulf Stream Ring, an energetic anticyclonic eddy is formed. This formation process and its eddy product have been observed several times [Gründlingh (1983) reviews the older observations, while Gordon *et al.* (1986) discuss a particularly detailed regional survey, and Bennett (1988) another]. An eddy thus formed initially contains in its core the water mass found on the offshore side of the Agulhas Current, while on the periphery, where the steep isopycnal slopes occur, it contains a ring of the Agulhas Current water mass formed by the pinched off segment of the Agulhas Current Retroflection. In the Retroflection sector of the Current the isopycnal slopes run deep, reaching to the sea floor (Jacobs and Georgi, 1977), so such an eddy could originate with a top-to-bottom dynamic signature.

In a synoptic survey of the entire region around South Africa, to 1500 m, Harris and van Foreest (1978) found the Retroflection centered at 21°E and 39°S, with a transport relative to 1100 db of about 35×10^6 m^3 s^{-1}. A Retroflection eddy therefore might be expected to begin its life with a transport of this magnitude. This same study also shows an anticyclonic eddy feature centered near 15°E and 36°S with an anticyclonic transport relative to 1100 db of $15–20 \times 10^6$ m^3 s^{-1}. The eddy observed on the 23°S section has a transport of about 15×10^6 m^3 s^{-1} relative to 1100 db (Table 1).

The more recent intensive Retroflection survey by Gordon *et al.* (1986) represents data from 14 years later, and from late spring rather than late fall, but nonetheless shows a quite similar field. The later realization of the general circulation field shows the dynamic height maximum defining the "center" of the Retroflection lying about 160 km west of and 80 km

south of its position in the earlier case. There is also a "Capetown eddy" at 35°S and 15°E, where HARRIS and VAN FOREEST (1978) reported their eddy. More hydrographic details are available in GORDON *et al.*'s (1986) study, which we will discuss in a later section. Here we note that the Capetown eddy had a single thermostad spanning depths from 40 to 265 m at a temperature of about 16.4°C, interpreted by the authors as a product of winter convection in the eddy core subsequent to its pinch-off. The Capetown eddy transport relative to 1500 db is 35×10^6 m^3 s^{-1}, considerably larger than our eddy's 19×10^6 m^3 s^{-1} (Table 1).

In the Gordon *et al.* survey, the primary anticyclonic eddy was found about 500 km west of the Retroflection (near 39°S and 18°E), and was apparently more recently formed by the pinch-off process than the Capetown eddy. The transport of this "Retroflection" eddy is 40×10^6 m^3 s^{-1} relative to 1500 db (equivalent to about half the Agulhas Current transport entering the Retroflection region from the east according to the authors). DUNCAN (1968, 1970) reported a similar Retroflection eddy 250 km WSW of the location of the Gordon *et al.* eddy, with a transport of 29×10^6 m^3 s^{-1} relative to 1000 db. VISSER (1969) in his treatment of the data set Duncan utilized, noted saline AAIW and UNADW within the eddy.

Yet another realization of the hydrographic fields of the Retroflection region was taken in late fall 1985 (BENNETT, 1988), and this data set also contained a Capetown eddy, centered at 35°S and 15°E, the same position as the other two realizations. This realization of the Capetown eddy had a transport of about 25×10^6 m^3 s^{-1} relative to 1500 db and did not contain a core of converted water. The Agulhas Retroflection was well west in 1985, with its pivot point near 38°S and 19°W, overlapping the area where the Gordon *et al.* survey two years earlier described the Retroflection eddy. This westward extension of the Retroflection, and the additional doming of the thermocline within the Retroflection near 24°E (BENNETT, 1988) could be an indicator of incipient formation of a Retroflection eddy.

OLSON and EVANS (1986) described the near-field propagation of the Gordon *et al.* eddy pair, based on satellite-tracked drifters deployed in the two features during the hydrographic cruise, on satellite infra-red imagery, and on analysis of the Gordon *et al.* hydrographic data. Both eddies were about 400 km in diameter (based on the depression of the 10°C isotherm), with maximum azimuthal speeds (by both gradient balance calculation and float observation) at a radius near 120 km (the XBT section, Fig. 4a, suggests that the maximum speed radius of our eddy was on the order of 100 km, as this is where the steepest isotherm tilts were observed). Both were interpreted to have a substantial barotropic circulation superimposed on the baroclinic field, that is, the float speeds were greater than those calculated by gradient balance relative to 10°C. Over the three months subsequent to the drifter deployments, the net translations of the two eddies were in the same overall direction, 29° north of west. The mean drift speed of the Capetown eddy was 4.8 cm s^{-1}, with a maximum average azimuthal speed of 60 cm s^{-1}, while the younger Retroflection eddy was more energetic, with a mean drift speed of 8.5 cm s^{-1}, and a maximum average azimuthal speed of 90 cm s^{-1}. These initial trajectories are basically orthogonal to the upper South Atlantic baroclinic field. Such trajectories would pass well south of our eddy's position at 23°S and 5°W. To cover the distance at the indicated translation speeds would take 1.2–2.2 years. If the eddies ceased propagating across the mean circulation streamlines and instead passively advected along the streamlines, they would arrive at 23°S, 5°W where we found the eddy. Subsequent observations (Fig. 5, kindly supplied by Olson, personal communication, 1986) confirm such a basic

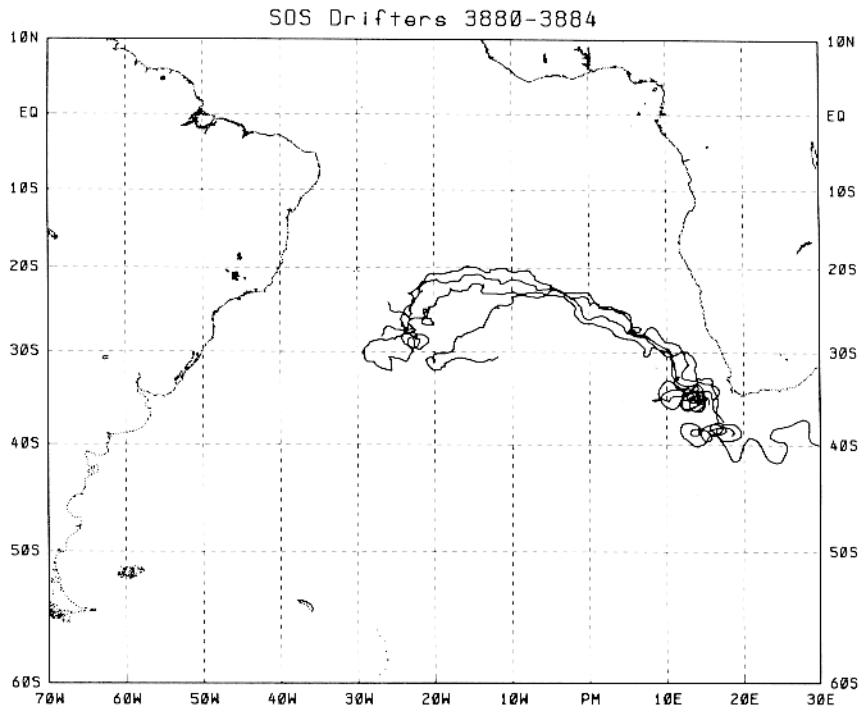

Fig. 5. Surface drifter trajectories, kindly given to the authors by Don Olson. Three of these were released in the Capetown eddy (Fig. 8), one in the Retroflection eddy (Fig. 10). Olson and Evans (1986) discuss in detail the behavior of these drifters while they were trapped in these eddies. The trajectories here include that early part, but are extended in time subsequent to the escape of the drifters from the eddies.

general circulation path: surface drifters deployed near Capetown drifted on a long, gently curving track consistent with the basin-scale baroclinic field (Fig. 6, from Reid, 1989) passing near our eddy observation site and continuing westward from there. These floats were the same ones that were seeded in the two eddies. The floats had escaped the eddies four months after deployment, as indicated by the cessation of circular trajectories superimposed on the general drift. Their mean translation speeds after escape were on the order of 5–10 cm s^{-1}.

Thus, the Agulhas Retroflection pinch-off mechanism with subsequent propagation into the eastern South Atlantic seems to be the most plausible for the origin of the eddy observed on the 23°S section.

E. Eddy generation at the Walvis Ridge

The Walvis Ridge connects Africa at 20°S to the Mid-Atlantic Ridge at 35–40°S, intersecting our 23°S section at 6°E. The Walvis Ridge crests at less than 3000 m depth almost everywhere, and has many segments significantly shallower. It is a major topographic feature that would disrupt a deep-reaching current that traverses the Ridge. If the eddy were formed in the Agulhas Current, then it must have transversed the Walvis Ridge.

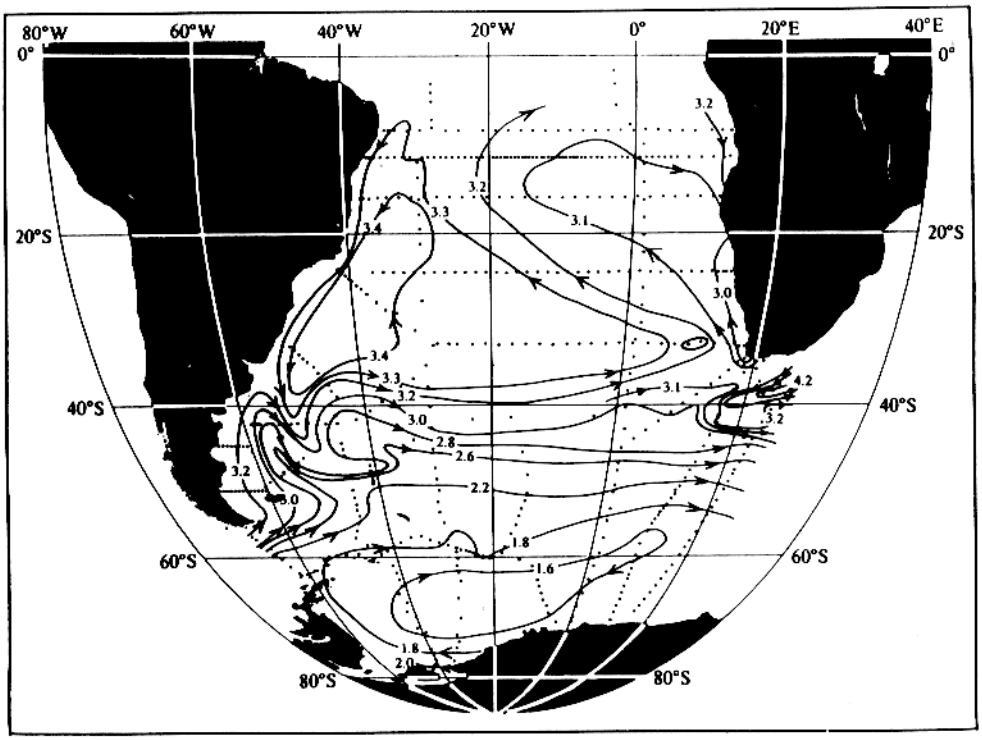

Fig. 6. Absolute steric height at the sea surface of the South Atlantic ocean, from REID (1989).

The Retroflection, the Retroflection eddy, the Capetown eddy, and our eddy all have dynamic signatures reaching depths exceeding the crest depth of the Walvis Ridge. This does not mean that such eddies cannot move across the Ridge, only that the deeper levels cannot. Any water mass deeper than the Ridge crest that might have been trapped within such an eddy at formation and was being carried with the drifting eddy would most likely be left behind at the Ridge, unless there was a large dynamic uplift associated with the Ridge traversal.

Figure 6 is a rendition of the absolute dynamic height at the sea surface from REID's (1989) study of the South Atlantic general circulation and it is structurally similar to the chart of 0/2000 db relative dynamic height difference used by OLSON and EVANS (1986) in developing their idea of Agulhas Retroflection eddies being carried by the mean general circulation to the spot of our observation. We make an additional point that, south of the latitude of southern Africa, the dynamic height contours are basically zonal, indicating the west-wind drift of the southern closure of the subtropical gyre and of the circumpolar current to its south. One might expect an evenly spaced northward "peeling" off of contours between South America and Africa indicative of an ocean-wide Sverdrup interior circulation. Instead, most of the northward flow is concentrated in a narrow band at the eastern boundary. This is the basis of GORDON's (1985, 1986) hypothesis of a warm-water pathway connecting the Indian and South Atlantic Subtropical regimes. The dynamic height also presents an image of the Benguela Current that is much more concentrated off Capetown than in our section farther north at 23°S.

This strong northwest flow into the South Atlantic interior could lead to eddy formation through interaction with the Walvis Ridge in two different ways. As the current traverses the Ridge, the topography could force meanders over the ridge or in its lee that could pinch off to form an eddy of either sign. We already have noted that the 23°S observations show deep density structure west of the Walvis Ridge which has a wavy character consistent with the image of lee meanders (and this is the location of the other observation of an eddy feature at Sta. 108). The other eddy formation mechanism at the Ridge would be somewhat larger scale. The South Atlantic dynamic height field exhibits a 135° anticyclonic turning of the flow from the eastward flow of the southern limb of the gyre to northwest flow over the Walvis Basin. It might be possible for topographic interaction to induce this current elbow to bend even farther, doubling back on itself to form an anticyclonic eddy by a pinch-off west of the elbow. In this case, the water mass initially trapped within the eddy would be the southeastern South Atlantic one. Such an origin for the waters trapped in the eddy, however, is not as consistent with the observations on the 23°S section as the origin in the Agulhas Retroflection region.

3. THE CAUSES OF THE WATER MASS ANOMALIES IN THE EDDY

Henceforth we adopt the Agulhas Retroflection hypothesis for the origin and generation mechanism for our eddy. We now attempt to explain the water mass anomalies of the eddy in the framework of this hypothesis.

The Capetown eddy observations (Gordon *et al.*, 1986) are helpful for the interpretation of the double thermostad in our eddy. These support the mechanism of convective overturning progressively modifying the trapped water mass in the eddy core, and through a net buoyancy loss producing thermostads. This is a familiar process from studies of the convective modification of the core of warm core rings of the Gulf Stream. Schmitt and Olson (1985) describe the evolution through summer of a warm-core Gulf Stream Ring found in late winter. Convection formed a 400-m thermostad at 15°C that progressively capped off in the spring and summer. Their density sections showed a reversal of isopycnal slope reminiscent of the shift from a bowl to a dome and the shear reversal in the 23°S eddy. The Capetown eddy had a thermostad at about 16.5°C reaching to about 250 m, with only a thin heated cap isolating it from the sea surface in this late spring data set (Fig. 7). This penetration depth is similar to the lower thermostad in the 23°S eddy, although the 23°S eddy thermostad is about 1°C cooler. The exact temperature attained would depend on the specifics of the individual eddy's life history.

Gordon *et al.* interpreted the Capetown eddy thermostad as a cooling-induced modification of the water mass found to the east of the retroflecting Agulhas Current. In that region the Agulhas Current has a mild thermostad at 17–18°C that seems to be a local version of Subtropical Mode Water (STMW, coincidentally at the same temperature as the archetypal variety in the North Atlantic). As is typical for mode waters, the temperature seems to be interannually persistent: a section across the Agulhas upstream from the Retroflection (Bennett, 1988) showed the identical thermostad two years later (Fig. 8). This mild thermostad also was observed within the Retroflection eddy (Fig. 9), reflecting its recent detachment from the Retroflection. It is also visible (Fig. 10) in the 1985 realization of the Capetown eddy (Bennett, 1988), suggesting that this Capetown eddy had not over-wintered as the 1983 one apparently had. Stations in the Capetown eddy

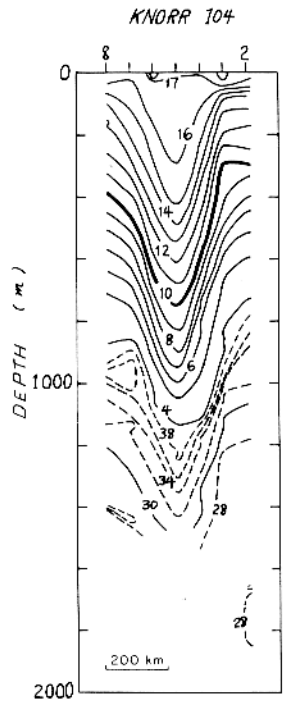

Fig. 7. Potential temperature distribution across the November 1983 Capetown eddy (GORDON *et al.*, 1986; data reported in CAMP *et al.*, 1986).

during late fall 1985 show considerable amounts of water warmer than 17°C that would have to be eroded away in winter to expose the STMW to convective overturning and additional cooling of the exposed thermostad to produce the cooler thermostad of the 1983 Capetown eddy, or the even cooler lower thermostad of our eddy. The 1983 Retroflection eddy core, believed to have been formed just prior to observation (GORDON *et al.*, 1986), contains the STMW thermostad, but with only a weak warmer cap in this spring data. GORDON (1985) has estimated that one year's local average annual heat flux to the atmosphere provides sufficient cooling to remove this warm cap and to penetrate through the STMW to produce the thermostad at 16.5°C observed in the Capetown eddy.

We hypothesize then that our eddy's early life history resembled the 1983 Capetown eddy, that it headed past Capetown toward the central South Atlantic, and that the thermostad became capped with stored heat in the next spring and summer heating phase. If one more seasonal cooling event occurred after this point before our mid-summer observation at 23°S, then the shallower thermostad in our eddy can be explained, provided only that the heat stored in the heating phase exceeded that removed during the second cooling phase. As the cooled Retroflection fragment is moved to lower latitudes and less cold climate, it might be expected that the drifting eddy would exhibit a net gain of heat. Also, the advection speeds noted earlier [OLSON and EVANS (1986)] are consistent with the notion of more than one winter transpiring between eddy formation and our observation at 24°S.

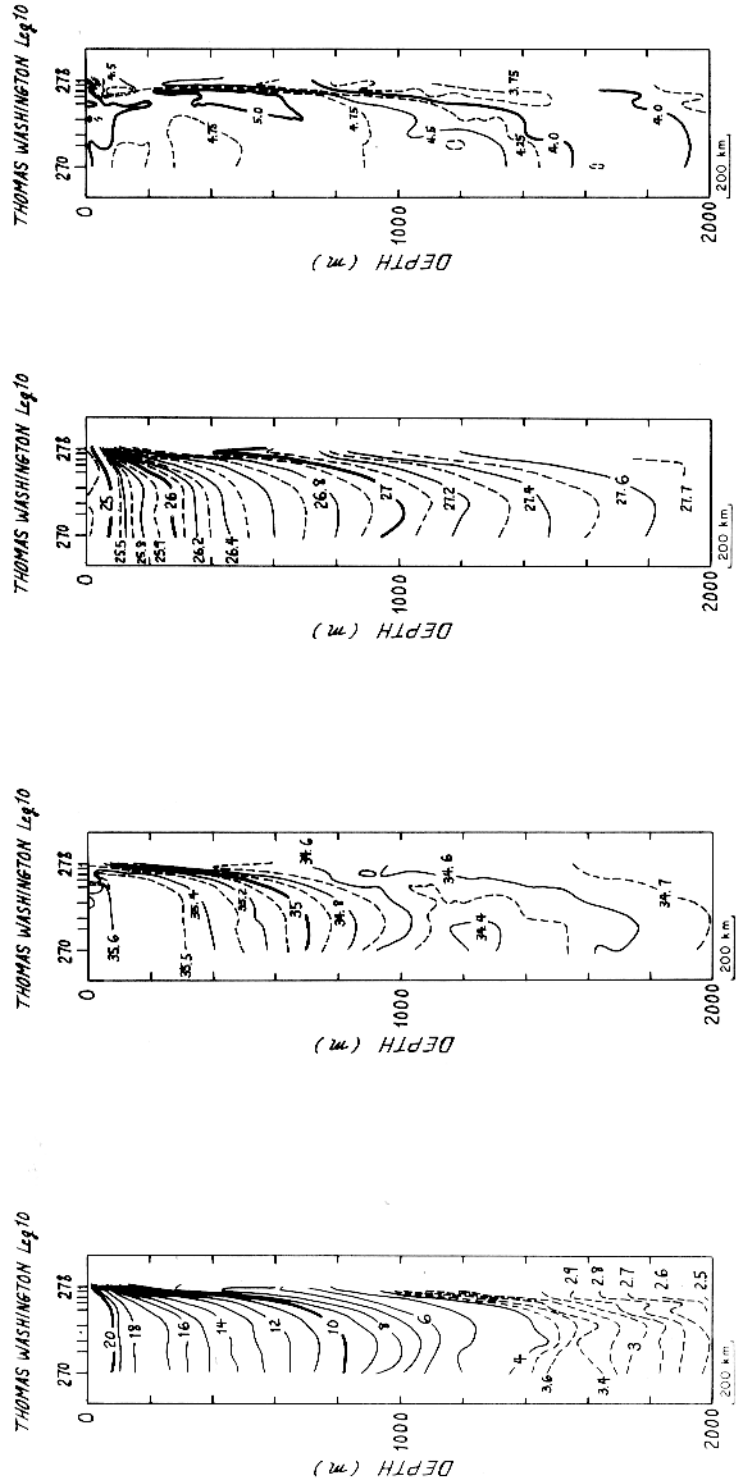

Fig. 8. Property distributions across the Agulhas Current at 25°E in March, 1985 (Bennett, 1988). (a) Potential temperature (°C); (b) salinity (psu); (c) potential density anomaly, referenced to 0 db (kg m^{-3}); (d) dissolved oxygen (ml l^{-1})

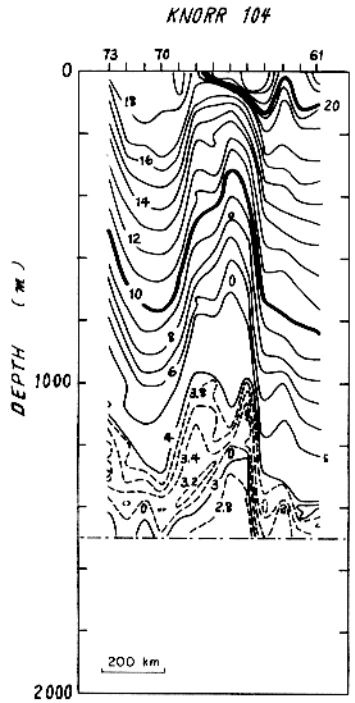

Fig. 9. Potential temperature distribution across the November 1983 Retroflection eddy (Gordon *et al.*, 1986; data reported in Camp *et al.*, 1986).

In the eddy core the next anomaly beneath the thermostads is extension of higher oxygen down into the thermocline, including a mild maximum near 13°C. The westernmost of the Indian Ocean varieties of Subantarctic Mode Water (SAMW, McCartney, 1977, 1982) have a temperature of about 13.5°C, while the total range of varieties recirculating within the Indian Ocean subtropical gyre interior west of Australia has temperatures from 13.5°C down to 8°C. The latter coldest varieties form near Australia and have the longest subtropical circulation path to carry their influence back west to the Agulhas. These modes provide a high-oxygen influence to this temperature range of the thermocline. The 1985 section (Bennett, 1988) across the Agulhas upstream of the Retroflection (Fig. 8) shows this SAMW high-oxygen influence defined by the 4.75 ml l^{-1} contour (spanning θ = 9–14°C) offshore, and more intense, ≥5.0 ml l^{-1}, contour within the core of the Current (centered on 12°C). Between this higher oxygen layer and the STMW thermostad is a lower oxygen layer centered near 15°C, which delineates the SAMW influence as an oxygen maximum layer. Beneath the high-oxygen core the oxygen basically decreases steadily to values lower than 4.0 ml l^{-1} beneath the core of the AAIW. There is only a slight oxygen maximum at the AAIW core superimposed on this decreasing trend, resulting in a weak oxygen minimum above the AAIW core near θ = 6°C. The thermocline oxygen structure of the Agulhas Current is thus a very good match to the core water mass of our eddy. The Agulhas Current does not, however, show a counterpart to the ring of low-oxygen thermocline water observed on the periphery of our eddy. This feature was centered on the 6–10°C temperature range. The Agulhas Current section

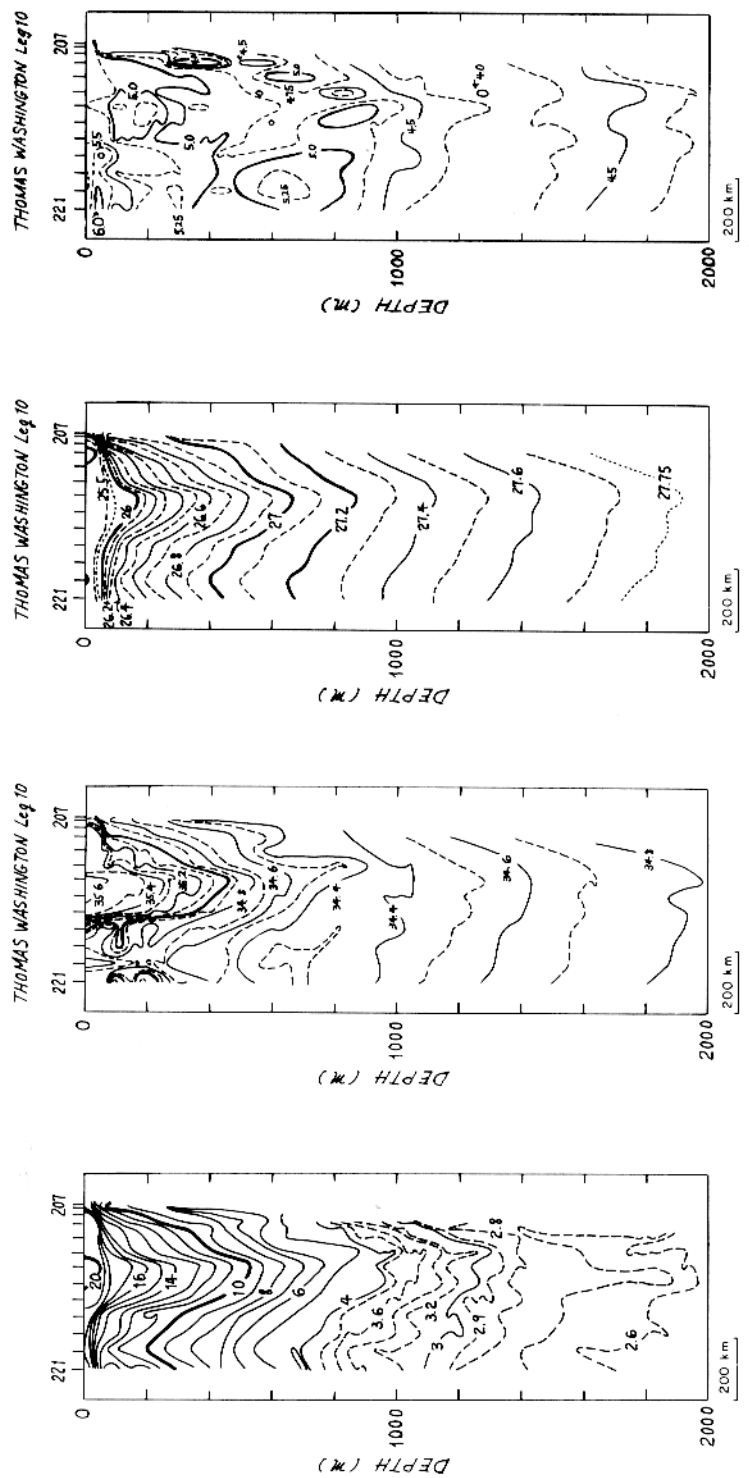

Fig. 10. Property distributions across the March 1985 Capetown eddy (Bennett, 1988). (a) Potential temperature (°C); (b) salinity (psu); (c) potential density anomaly, referenced to 0 db (kg m^{-3}); (d) dissolved oxygen (ml l^{-1}).

exhibits generally lower oxygen levels throughout the thermocline on the onshore side of the Current, but without a minimum at that temperature range.

In the eddy, the next feature down in the anomaly stack is the AAIW, which appeared doubly anomalous in the core of our eddy: more saline than that in the surrounding stations, and with distinctly lower oxygen levels, visually dominated by the pronounced minimum layer just beneath the salinity minimum core of the AAIW. The AAIW of the subtropical gyre of the southwestern Indian Ocean is more saline and less highly oxygenated than in the southeastern South Atlantic. The Agulhas Current section (Fig. 8) shows the AAIW within the Agulhas Current core to be very saline, defined by a salinity minimum less than 34.6 or 34.5 psu. Offshore the minimum is more pronounced, falling below 34.4 psu. As noted above, the oxygen decreases from the overlying maximum of the SAMW through the AAIW core down to a minimum (≤ 4 ml l^{-1}) in the lower AAIW at a temperature of about 3.6–3.8°C. This minimum oxygen layer is more pronounced onshore where the salinity minimum is more saline. While the overall properties of the AAIW in the Agulhas Current are similar to those of the AAIW in the core of our eddy, we note that there are problems with the details of the AAIW distribution. If the Agulhas Current (Fig. 8) were folded around to form an eddy, the more saline and less oxygenated AAIW would be at the periphery not in the core, which is opposite to what we observed in the eddy.

Beneath the AAIW, the eddy at 5°W, 23°S showed UNADW with slightly elevated salinity ($\geq$34.88 psu). The Agulhas Current data shows UNADW with salinity levels on the order of 0.05 psu lower than this (BENNETT, 1988), the Agulhas Current water mass does not appear to be the source of this feature.

The thermostads and the main thermocline anomalies in the eddy center seem amenable to explanation as trapped waters from the Agulhas Current, with subsequent convective modification causing the former. The anomalies at AAIW and UNADW levels, and the ring of low oxygen surrounding the eddy at main thermocline depth are not amenable to the same explanation. The key to the explanation of these remaining water masses lies in the kinematics of propagating eddies. There is a large and growing literature on the dynamics of strong eddies, but here we will focus on the general kinematic concept of trapping without drawing on a specific dynamic model.

A study by FLIERL (1981) is particularly useful, and we show in Fig. 11 some graphical results from this work. He calculates the paths that fluid particles follow as an eddy moves through a region. There are two types of paths, closed loops corresponding to particles trapped in and moving with the eddy (dashed curves 9 and 10 of Fig. 11a), and meanders corresponding to a disturbance to the particle position induced by the passage of the eddy (dashed curves 6, 7 and 8 in Fig. 11a and the particle paths of Fig. 11c). A critical parameter determines whether a trapped region exists at a given depth and, if so how large it is, and how extensive the induced disturbance is. The parameter is the ratio of the maximum azimuthal speed at the depth in question to the eddy drift speed, Flierl's ε parameter. The trapping only occurs in the depth range where $\varepsilon < 1.0$; in the example in Fig. 11 $\varepsilon = 1.75$. Flierl gives explicit formulas for the geometry of the trapped region and the extent of the induced disturbance. Some of these are included in Fig. 11b; the distance is scaled such that one unit corresponds to the radius of maximum azimuthal speed; the eddy is modeled (after OLSON, 1980) as rigidly rotating inside this radius, and with a exponential decay, $\exp[-r + 1]$, outside this radius.

In the present context these images correspond to a southern hemisphere anticyclonic eddy moving westward relative to the water column in which it resides. The eddy

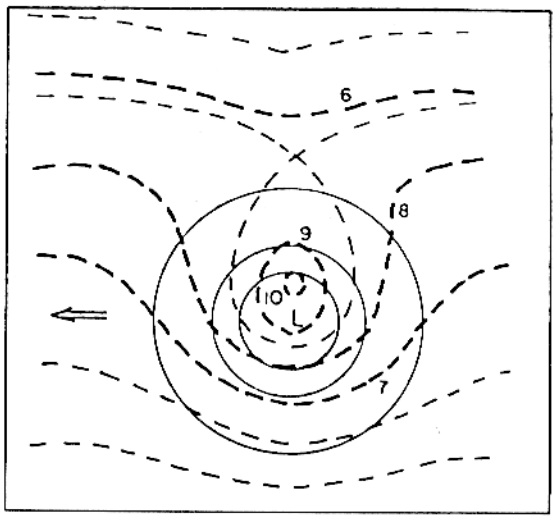
6
8
9
10
7

(a)

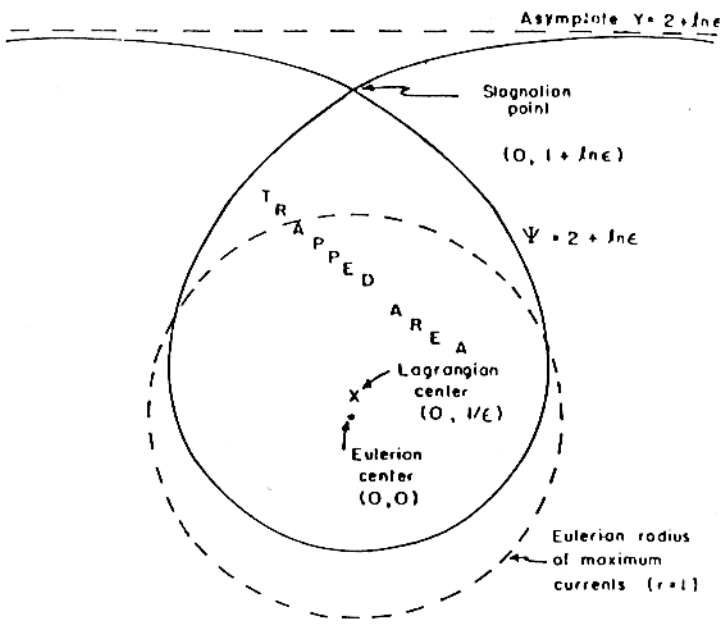
Asymptote Y = 2 + ln ε
Stagnation point
(0, 1 + ln ε)
Ψ = 2 + ln ε
TRAPPED AREA
Lagrangian center
(0, 1/ε)
Eulerian center
(0,0)
Eulerian radius of maximum currents (r = 1)

(b)

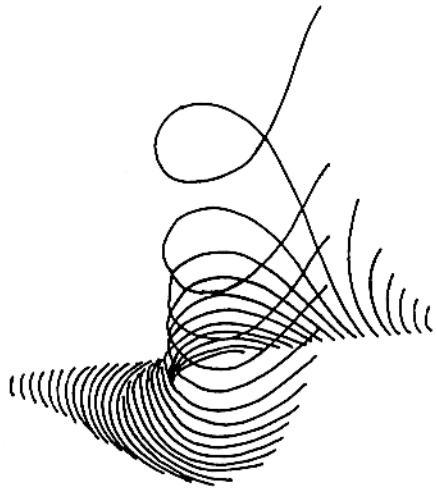

(c)

Fig. 11. From FLIERL (1981). The fields are computed for a northern hemisphere cyclonic (counterclockwise) eddy drifting westward (north is the positive "y" direction). They also correspond to a southern hemisphere anticyclonic (counterclockwise) eddy drifting westward (still with north as the positive "y" direction). (a) The solid concentric circles are the instantaneous stream-function of the axisymmetric eddy. The dashed contours are the steady stream-function contours in the reference frame moving with the eddy. Centered north of eddy center is a teardrop-shaped closed contour that defines the trapped region. On and inside this contour, particles, which follow the dashed streamlines, move in closed loops like curves 9 and 10. Particles starting at latitudes well north of the trapped region, like curve 6, are deflected momentarily toward the eddy as it passes and, as indicated by the difluence of streamlines, are displaced in the direction of the eddy's motion. Particles that start in the latitude range of the eddy, like curves 7 and 8, are pulled around the southern side of the trapped region, and thus momentarily deflected over a larger latitude range than those further north (or south). These particles experience a net displacement in the opposite direction to the eddy's propagation, due mainly to the large speeds associated with the confluence of streamlines to the south of the trapped region. (b) Geometry of the trapped region, with key distances expressed in terms of ε, the ratio of the maximum azimuthal speed to the drift speed. The sketch corresponds to $\varepsilon = 1.75$, as does the detailed field of Fig. 11a. The trapped area goes to zero at $\varepsilon = 1.0$. (c) Displacements of particles initially evenly spaced along a meridian induced by the westward passage of the ring illustrated in Fig. 11a, viewed in the ocean reference frame. The looping of water around the trapped core is particularly evident.

azimuthal velocity has vertical shear; its drift speed is taken as barotropic. For the former we use the velocity profiles of Fig. 3, and the higher resolution (XBT) section of Fig. 4a suggests an eddy radius of at least 90 km (we may not have crossed the eddy at dead center, of course, which would affect both the apparent diameter and the maximum speed estimate). OLSON and EVANS (1986) found this radius to be 120 km for the Capetown eddy, while the velocity section across an eddy at 8°E and 29°N recently described by GORDON and HAXBY (1990) indicates a radius of 130 km. For simplicity we will adopt a radius of 1° of latitude, so the distances in Fig. 11 and Flierl's formulas can be viewed as in units of degrees. The drift speed is not known; we use two estimates for illustration, 5 and 10 cm s^{-1}. These bracket the speeds of the Capetown and Agulhas eddies reported by OLSON and EVANS (1986), and the range 5–8 cm s^{-1} inferred by GORDON and HAXBY (1990) from analysis of satellite altimetry data. We have provided a second axis label for the speed

profiles of Fig. 3, for converting the speeds to Flierl's ε parameter, using these two drift-speed estimates.

In a reference frame moving with the steadily translating eddy, the particle paths at a given depth are a superposition of the axisymmetric streamlines of the eddy's azimuthal circulation at that depth and a uniform approaching flow with a speed equal to the eddy drift speed. In this reference frame all particles shift southwards as the eddy approaches, and slow their approach in the north, where the azimuthal and drift speeds are subtractive, and accelerate to the south where the speeds are additive. In the Eulerian frame (Fig. 11c) particles initially at latitudes north of the eddy exhibit net westward displacements, a Lagrangian drift induced by the eddy passage, while those initially to the south exhibit net eastward displacements.

At depths where $\varepsilon < 1.0$ there is no trapped region in the eddy, and only the induced disturbance occurs, with a maximum deflection of particles southward towards the eddy of less than one eddy radius. For $\varepsilon = 1$ a stagnation point occurs: a degenerate trapped region of zero area located at the radius of maximum azimuthal speed at the north side of the eddy. Particles at the stagnation point in this case have been pulled southwards towards the eddy a distance of one eddy radius; all other particles exhibit southward deflections less than this distance. For $\varepsilon > 1$ the trapped region is of non-zero area, and is a teardrop shape centered to north of the eddy center. This trapped region extends north of the radius of maximum azimuthal speed by a scaled distance $\ln\varepsilon$ (that is from a distance $1 + \ln\varepsilon$ from eddy center). Particles from as far north of the north edge of the eddy as $1 + \ln\varepsilon$ units (that is from a distance of $2 + \ln\varepsilon$ from the eddy center) are pulled anticyclonically around the trapped region. The larger the ε value, the larger the trapped area and the more distant the origin of particles pulled around the trapped core.

Using the ε annotated axis in Fig. 3, the critical value of $\varepsilon = 1.0$ is reached at a depth of about 1100 m for the slower drift speed, and about 670 m for the faster drift speed. These are then our estimates for the depth of penetration of the trapped region, that is the depth at which the area of trapping goes to zero. At that depth, water from as far as one eddy diameter to the north of the eddy center would be pulled south to the edge of the eddy. Smaller southward deflections would occur deeper in the water column where $\varepsilon < 1$. Table 2 summarizes some geometric aspects of the trapped region in the upper water column, and the extent of the southward displacement of particles throughout the upper 1500 m. At the level of the thermostads the trapped area is probably at least as large as the eddy, and possibly as much as almost three times that area. Particles normally resident as far as 3 or 4° north of the eddy center would be pulled anticyclonically around this large trapped region. At main thermocline levels the trapped area is less extensive, but substantial southward movement of particles still occurs, with particles from perhaps two or three degrees north of the eddy pulled around the trapped core. We believe that this is the explanation of the ring of low oxygen we observed at thermocline depths on the periphery of our eddy. Figure 12a,b shows the potential temperature and oxygen distribution along a meridional section near the Greenwich Meridian (Reid, 1989). Northward from 30°S, the mid-thermocline oxygen minimum intensifies, and the underlying AAIW oxygen maximum weakens, and at Sta. 32 (at 24°S, the intersection with the *Oceanus* section five months earlier, Fig. 2) the minimum layer broadens, the AAIW oxygen maximum disappears, and oxygens are less than 4.0 ml l^{-1} for temperatures between 4 and 10°C. Reid's charts show property isolines in this area oriented about 20 or 30° south of east, so the transition to low oxygen that occurs at 24°S along the Greenwich meridian (Fig. 12b) might be expected to lie 200 or

300 km farther north at the longitude of our eddy (nominally 5°W). We thus explain the ring of low oxygen surrounding the core of our eddy as a "streamer" of lower thermocline oxygen normally found an eddy-diameter or so further north, that has been pulled southward around the trapped Agulhas Current water in the core of the eddy, like streamline 8 in Fig. 11a.

Due to the decay of the eddy azimuthal speed with depth, the area of closed particle paths (trapped water moving with the eddy) decreases with depth, until near the depth where this maximum azimuthal speed has fallen to the drift speed, it vanishes, and none of the particle paths close (Table 2). At this depth and below, particles shift southward as the eddy passes over then return to their original position, with a displacement of roughly an eddy-diameter at the level where the speeds are equal, but a smaller displacement deeper where the eddy speeds decay even further. This pattern explains the AAIW and UNADW characteristics that we observed in the deep footprint of the 23°S eddy. The meridional sections along the Greenwich Meridian (REID, 1989) show the salinity maximum of the UNADW increasing northward (Fig. 12c), with accompanying decreases in nitrate (Fig. 12d) and silicate (Fig. 12e) at their associated minima. The AAIW salinity minimum also weakens northward, with the sharp change in its oxygen content just noted. These water

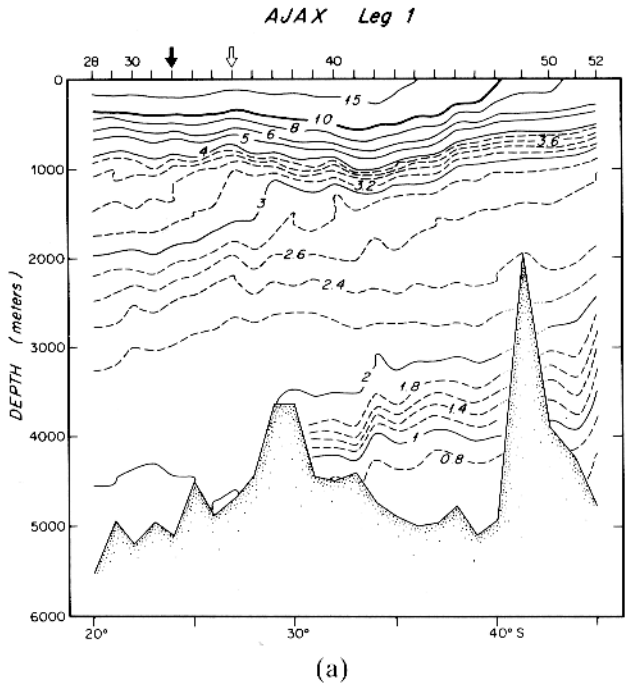

(a)

Fig. 12. Property distribution nominally along the Greenwich Meridian, Ajax Expedition leg 1, R.V. *Knorr* Cruise 104, leg 4, October–November 1983, data from Reid (personal communication 1987, discussed in REID, 1989). Transect position in Fig. 1. The heavy arrow indicates the latitude where the eddy was observed 600 km to the west. The light arrow farther south reflects the expected impact of the non-zonality of thermocline water mass isolines (TSUCHIYA, 1986; REID, 1989): the water mass distribution at 23°S, 9°E might be expected to be more closely related to that at 27°S along this section than at 23°S along the section. (a) Potential temperature (°C).

(*Continued overleaf*)

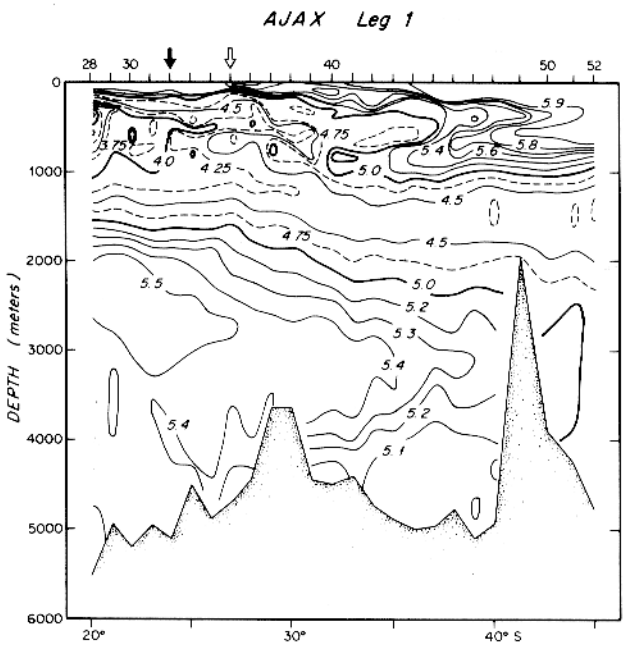

(b)

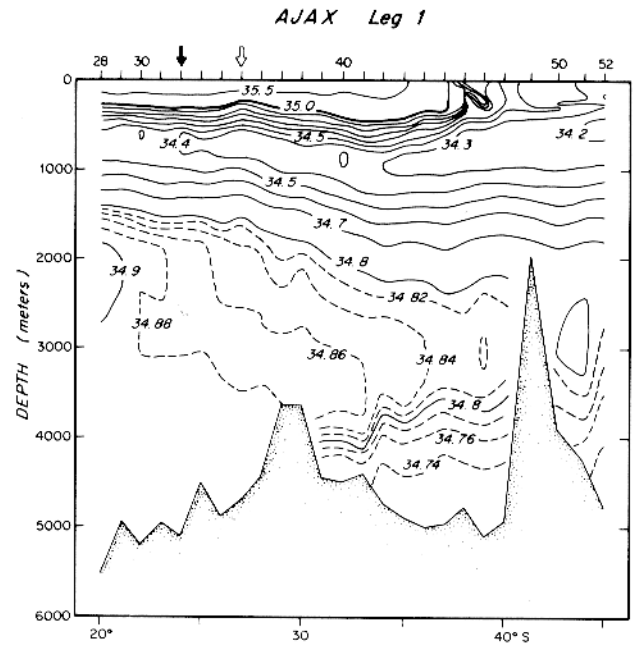

(c)

Fig. 12 *continued*. (b) Dissolved oxygen (ml l^{-1}). A low oxygen ring (Fig. 4e) surrounded the eddy at thermocline temperature, and low oxygen AAIW was found beneath the eddy. Both these features are seen here at Sta. 31 and farther north. (c) Salinity (psu). A ≥ 34.88 psu maximum appeared in isolation beneath the eddy (Fig. 2b) as did a more saline variety of AAIW. Both these features are seen here at Sta. 31 and farther north.

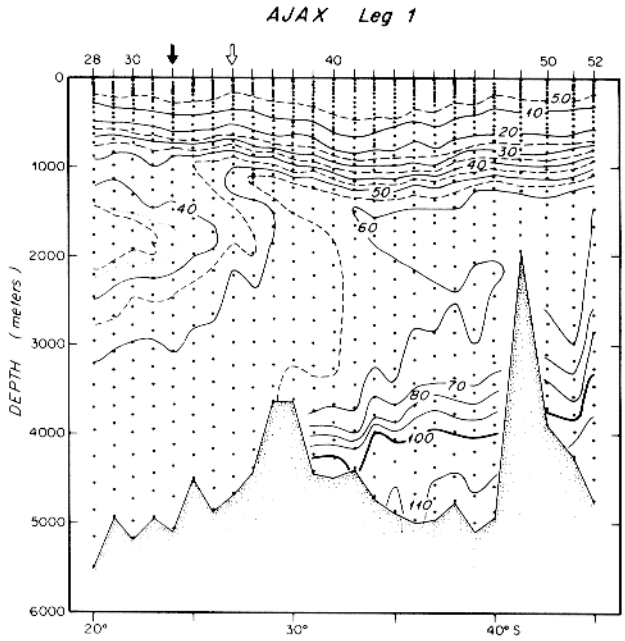

(d)

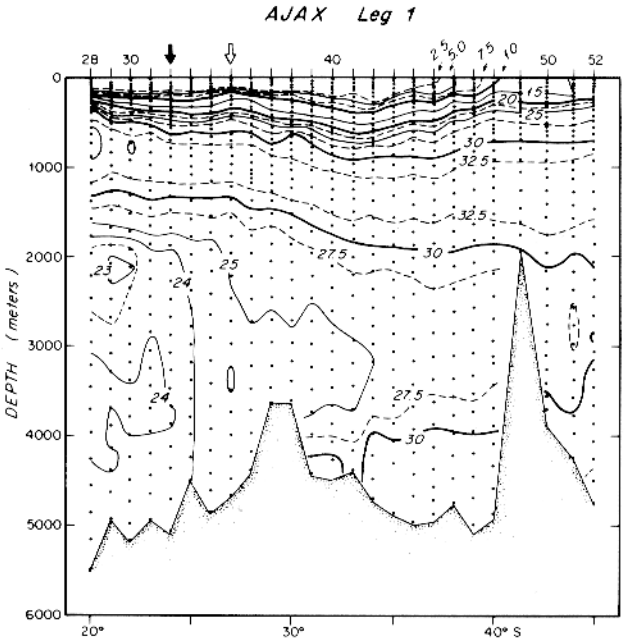

(e)

Fig. 12 *continued*. (d) Silicate (μmol l^{-1}). A slightly lower silicate minimum in the UNADW was observed beneath the eddy at 2000 m (Fig. 2e). This feature is seen here at Sta. 32 and farther north. (e) Nitrate (μmol l^{-1}). A slightly lower nitrate minimum was observed beneath the eddy at 2200 m. This feature is seen here at Sta. 30 and farther north.

Table 2. Estimated parameters for the trapped region of the eddy (see text)

Depth (m)	Maximum azimuthal speed (cm s^{-1})	Drift speed (cm s^{-1})	Ratio of maximum azimuthal speed to drift speed ε	Asymptote $2 + \ln\varepsilon$	Stagnation point $1 + \ln\varepsilon$	Lagrangian center ε^{-1}	Area
0	26.8	5	5.4	3.7	2.7	0.19	2.6
		10	2.7	3.0	2.0	0.37	1.1
150	27.9	5	5.6	3.7	2.7	0.18	2.7
		10	2.8	3.0	2.0	0.36	1.1
500	16.4	5	3.3	3.2	2.2	0.30	1.6
		10	1.6	2.5	1.5	0.63	0.4
800	7.6	5	1.5	2.4	1.4	0.67	0.4
		10	0.8	*	*	*	*
1000	5.6	5	1.1	2.1	1.1	0.91	0.1
		10	0.5	*	*	*	*
1500	2.6	5	0.5	*	*	*	*
		10	0.3	*	*	*	*

*Indicates that the eddy azimuthal speed at the depth is not large enough to cause a trapped region to form.

masses normally found to the north of the eddy location, then, have been pulled southward under the eddy as it passed by.

There remains an ambiguity for the AAIW distribution: does any of this water mass within the eddy represent trapped water from the Agulhas Current? We cannot be conclusive, for the AAIW north of 24°S in the central South Atlantic and in the Agulhas Current are too similar in their water mass characteristics. The 1983 (Fig. 7) and 1985 (Fig. 10) realizations of the Capetown eddy suggest that some degree of trapping of AAIW occurs in this earlier phase of the eddy history. Both these sections run southwest out of Capetown, and thus cross the expected drift direction at more or less right angles. A section across the theoretical eddies of Fig. 11 at right angles to the drift direction, i.e. north–south, indicates that the trapped region would be found to the Capetown side of the eddy center. In both Capetown eddies, low-salinity, high-oxygen AAIW is found at eddy center and to the southwest (Stas 5, 6 and 7, Fig. 7; and 215, 216, 217 and 218, Fig. 10), while the first station to the northeast of eddy center (Sta. 4, Fig. 7; and 214, Fig. 9) has higher salinity, lower oxygen AAIW. So in the initial movement of Retroflection eddies toward the northwest, there is a core of Agulhas Current AAIW trapped within them.

4. DISCUSSION

The hypothesis that the eddy at 5°W, 23°S originates by a barotropic pinch-off of the Agulhas Retroflection has a number of consistencies. The transport magnitude of the Agulhas Retroflection is of the same magnitude as that of the eddy, and there are now several examples of anticyclonic eddies near the Retroflection with diameters similar to the eddy at 23°S. There is a mechanism that is familiar: a large-amplitude disturbance to a western-boundary current produces a closed ring of the Boundary Current water mass with a core of the subtropical gyre water in the center. The eddy subsequently propagates

westward (either actively or by passive advection by the ocean interior circulation). The principal wrinkle for the present case is geometric. The familiar anticyclonic eddies in subtropical systems have a restricted region to move in, being constrained to the slopewater-type regions between a separated western-boundary current and the basin western boundary. As the Retroflection occurs south of Africa, the western boundary is absent, and the eddy can roam over the much larger domain of the South Atlantic interior. The openness of the domain may account for the evident longevity of the 23°S eddy, with the double thermostad and the advection speed estimates both suggesting a two-year life span. The Agulhas Current water mass provides a good match to the main thermocline water mass within the core of our eddy. Finally, the water mass properties such as the ring of low oxygen at thermocline levels that surrounds the core of the eddy, the distribution of AAIW in the core and the periphery of the eddy, and the indications of strengthened UNADW in the deeper reaches of the eddy can be explained in the context of recent theories of trapping regions within large eddies, and the disturbance to nearby water mass distributions induced by their propagation.

An active research topic is the amount of exchange of water between the Indian and South Atlantic Oceans (Gordon, 1985, 1986; Olson and Evans, 1986; Bennett, 1988; Rintoul, 1988). Two modes could contribute to such exchange: the mean currents and eddy exchange. The persistent occurrence of a Capetown eddy makes the estimation of the mean currents problematic, as the eddy seems clearly part of the time-mean picture, yet the net transport to the northwest past Capetown is presumably a fraction of the anticyclonic flow around an eddy that dominates each snapshot.

To the extent that we have satisfied the reader as to the origin of the eddy at 23°S, it is an energetic example of an eddy originating in the Indian Ocean making its way far into the South Atlantic Ocean. It is easy, however, to overestimate the volumetric impact of the eddy because of its extensive dynamic signature. As a dynamic entity, the eddy is approximately a column 400 km in diameter and 4.5 km high with a volume of 0.56×10^6 km^3. If one column of Indian Ocean water of this size entered the south Atlantic per year, it would correspond to a volume flux of 18×10^6 m^3 s^{-1}! The discussion of drifting eddy kinematics of the preceding section indicates that the trapped Indian Ocean water moving with the eddy at the time of observation is much smaller than the volume of the full eddy column. Using area numbers from the theoretical argument, we estimate the trapped "cone" of water at 0.036×10^6 km^3 (slow drifting eddy) to 0.013×10^6 km^3 (fast drifting eddy). One eddy per year with these trapped volumes corresponds to a volume flux of $1.1\text{–}0.4 \times 10^6$ m^3 s^{-1}. Even if the column estimates represent the eddy volume at formation, most of the Indian Ocean water will be left behind at the point of origin as the eddy begins to move relative to its surroundings. Olson and Evans (1986) noted that the drift speeds seem faster for younger eddies. As this means smaller values for ε, the stripping away of the Agulhas waters may be very substantial.

Gordon and Haxby (1990) interpret altimeter measurements as indicating perhaps five eddies per year entering the South Atlantic from the southeast and drifting across the Ocean at speeds of 5–8 cm s^{-1}. They estimate each eddy to represent a vertical column of Indian Ocean Water 380 km in diameter reaching over 1000 m in depth, giving a volume flux of 3×10^6 m^3 s^{-1} per eddy, or 15×10^6 m^3 s^{-1} for the five per year. While the size may be indicative of the Indian Ocean Waters at the point of formation, it will no longer be so after the eddy has drifted a diameter or two, as much of that water will be left behind. Their eddy diameter is not the diameter of maximum azimuthal speed, but instead the larger diameter at which the eddy shear signature disappears. Using our trapped cone estimates

above, a better estimate of the volume flux that five eddies per year represents is $2–5.5 \times 10^6$ m^3 s^{-1}.

We conclude by noting that the formation of an anticyclonic eddy to the west of a western boundary current and its subsequent emigration to the neighboring ocean to the west, is probably unique to the Indian and South Atlantic Oceans. South America extends much farther south than South Africa, and the western boundary current immediately north of the tip of South America is the north-flowing Falkland Current, with the south-flowing Brazil Current turning eastward almost 15° of latitude farther north. There does not seem to be any evidence for any type of eddy formed by either of these currents making its way into the South Pacific through Drake Passage. A similar situation exists at New Zealand. The south-flowing North Cape Current turns eastward at 42°S, and from there to the south tip of New Zealand the western boundary current is the north-flowing Southland Current. We know of no evidence that eddies from either of these currents move around the south tip of New Zealand into the Tasman Sea. Lastly, the East Australian Current turns eastward in the general neighborhood of 35°S, and although it exhibits lots of eddies, sometimes being characterized as a field of eddies instead of a mean current, we know of no evidence for any of these eddies making their way to the south of Tasmania.

Acknowledgements—The authors would like to thank D. Olson for generously supplying us with the drifter tracks plotted in Fig. 5; C. Collins for obtaining XBT probes to supplement our CTD sampling and working on the above data to produce the combined CTD/XBT section of Fig. 4; J. Toole and Sara Bennett for the use of their Agulhas survey data (Figs 8 and 10), funded by ONR contract N00014-82-C-0019, NR 083-004; A. Gordon for the use of his Agulhas survey data (Figs 7 and 9), funded by ONR contract N0001484-C-0132; Joe Reid for the use of his AJAX data (Fig. 12); and Glenn Flierl for permission to use the materials of Fig. 11. The collection of the Brazil Current data was funded by ONR contract N00014-82-C-0019, NR 083-004. The collection and analysis of the 23°S section and the preparation of this paper were funded by NSF grants OCE 78-22223, OCE 86-01017, and OCE 86-14486. We particularly thank the crew of the R.V. *Oceanus* for their fine performance in the lengthy cruise 133 in 1983. Ruth Gorski and Teresa Turner provided much-valued assistance in assembling all these materials and preparing the analysis products, while Anne-Marie Michael suffered valiantly through the senior author's handwriting to produce the manuscript. The present study is WHOI Contribution No. 7182.

REFERENCES

Bennett S. L. (1988) Where three oceans meet: the Agulhas Retroflection region. Ph.D. Dissertation, WHOI/MIT Joint Program in Oceanography, WHOI Report No. WHOI-88-51, 367 pp.

Camp D. B., W. E. Haines, B. A. Huber, S. E. Rennie and A. L. Gordon (1986) Agulhas Retroflection Cruise. Lamont-Doherty Geological Observatory Technical Report LDGO-86-1.

Duncan C. P. (1968) An eddy in the subtropical convergence southwest of South Africa. *Journal of Geophysical Research*, **73**, 531–534.

Duncan C. P. (1970) The Agulhas Current. Doctoral Dissertation, University of Hawaii, 76 pp. (unpublished manuscript).

Flierl G. R. (1981) Particle motions in large-amplitude wave fields. *Geophysical and Astrophysical Fluid Dynamics*, **18**, 39–74.

Fuglister F. C. (1960) *Atlantic ocean atlas of temperature and salinity profiles and data from the international geophysical year of* 1957–1958. Woods Hole Oceanographic Institution Atlas Series 1, 209 pp.

Gordon A. L. (1985) Indian–Atlantic transfer of thermocline water at the Agulhas Retroflection. *Science*, **227**, 1030–1033.

Gordon A. L. (1986) Inter-ocean exchange of thermocline water. *Journal of Geophysical Research*, **91**, 5037–5046.

Gordon A. L. and W. F. Haxby (1990) Agulhas eddies invade the South Atlantic—evidence from GEOSAT altimeter and shipboard CTD. *Journal of Geophysical Research*, **95**, 3117–3125.

GORDON A. L., J. R. E. LUTJEHARMS and M. E. GRÜNDLINGH (1986) Stratification and circulation at the Agulhas Retroflection. *Deep-Sea Research*, **34**, 565–599.

GRÜNDLINGH M. L. (1983) Eddies in the southern Indian Ocean and Agulhas Current. In: *Eddies in marine science*, A. R. ROBINSON, editor, Springer, Berlin, pp. 245–264.

HARRIS T. F. W. and D. VAN FOREEST (1978) The Agulhas Current in March 1969. *Deep-Sea Research*, **25**, 549–561.

HART T. J. and R. I. CURRIE (1960) The Benguela Current. *Discovery Reports*, **31**, 123–298.

HEEZEN B. C. and M. THARP, scientific co-ordinators (1978) General bathymetric chart of the oceans (GEBCO), Sheet 5.12., Canadian Hydrographic Service, Ottawa.

JACOBS S. S. and D. T. GEORGI (1977) Observations on the southwest Indian Ocean. In: *A voyage of discovery: George Deacon 70th anniversary volume*, M. V. ANGEL, editor. Supplement to *Deep-Sea Research*, Pergamon Press, Oxford, pp. 43–84.

JOYCE T. M. (1981) The influence of the mid-Atlantic Ridge upon the circulation and the properties of the Mediterranean Water southwest of the Azores. *Journal of Marine Research*, **39**, 31–52.

LEETMAA A. (1977) Effects of the winter of 1976–1977 on the Northwestern Sargasso Sea. *Science*, **198**, 188–189.

MCCARTNEY M. S. (1977) Subantarctic Mode Water. In: *A voyage of discovery: George Deacon 70th anniversary volume*, M. V. ANGEL, editor. Supplement to *Deep-Sea Research*, Pergamon Press, Oxford, pp. 103–119.

MCCARTNEY M. S. (1982) The subtropical recirculation of Mode Waters. *Journal of Marine Research*, Supplement to **40**, 427–464.

OLSON D. B. (1980) The physical oceanography of two rings observed by the cyclonic ring experiment. Part II, dynamics. *Journal of Physical Oceanography*, **10**, 514–528.

OLSON D. B. and R. H. EVANS (1986) Rings of the Agulhas Current. *Deep-Sea Research*, **33**, 27–42.

REID J. L. (1981) On the mid-depth circulation of the world ocean. In: *Evolution of physical oceanography, scientific surveys in honor of Henry Stommel*, B. A. WARREN and C. WUNSCH, editors, MIT Press, Cambridge, Massachusetts, pp. 70–111.

REID J. L. (1989) On the total geostrophic circulation of the South Atlantic Ocean: flow patterns, tracers, and transports. *Progress in Oceanography*, **23**, 149–244.

RINTOUL S. R. (1988) Mass, heat and nutrient fluxes in the Atlantic Ocean determined by inverse methods. Ph.D. Dissertation, WHOI/MIT Joint Program in Oceanography, WHOI Report No. WHOI-89-6, 286 pp.

SCHMITT R. W. and D. B. OLSON (1985) Wintertime convection in warm-core rings: thermocline ventilation and the formation of mesoscale lenses. *Journal of Geophysical Research*, **90**, 8823–8837.

TSUCHIYA M. (1986) Thermostads and circulation in the upper layer of the Atlantic Ocean. *Progress in Oceanography*, **16**, 235–267.

VISSER G. A. (1969) Hydrololgical observations in the southeast Atlantic Ocean. 1. The Schmidt-Ott Seamount area. Investigational Report 77, Division of Sea Fisheries, Department of Industries, Republic of South Africa, 23 pp.

WARREN B. A. (1981) Deep circulation of the world ocean. In: *Evolution of physical oceanography, scientific surveys in honor of Henry Stommel*, B. A. WARREN and C. WUNSCH, editors, MIT Press, Cambridge, Massachusetts, pp. 6–41.

WARREN B. A. and K. G. SPEER (1991) Deep circulation in the eastern South Atlantic Ocean. *Deep-Sea Research*, **38** (Suppl.), S281–S322.

WORTHINGTON L. V. (1972) Anticyclogenesis in the oceans as a result of outbreaks of continental polar air. In: *Studies in physical oceanography—a tribute to Georg Wüst on his 80th birthday*, A. L. GORDON, editor, Gordon and Breach, New York, **1**, 169–178.

WORTHINGTON L. V. (1977) Intensification of the Gulf Stream after the winter of 1976–77. *Nature*, **270**, 415–417.